

https://dspace.org/

Mine aftershocks and implications for seismic hazard assessment

Kgarume, Thabang Ephraim

2011-03-31
http://hdl.handle.net/10539/9293

Downloaded from a DSpace repository. https://dspace.org/



MINE AFTERSHOCKS AND IMPLICATIONS FOR SEISMIC HAZARD ASSESSMENT

Thabang Ephraim Kgarume

A dissertation submitted to the Faculty of Science, University of the Witwatersrand, Johannesburg, in fulfilment of the requirements for the degree of Masters of Science

Johannesburg, 2010

DECLARATION

I declare that this thesis is my own, unaided work. It is being submitted for the degree of Masters of Science in the University of the Witwatersrand, Johannesburg. It has not been submitted before for any degree or examination in any other University.

_____

(Signature of candidate)

_____ day of _____ 20____

To my late mother

Maureen Manne

1961 - 1987

PREFACE

This work was initiated as one of the outputs of the “Minimising the rockburst risk” project (SIM050302) of the Mine Health and Safety Council. The work was motivated by an incident which occurred in a deep South African gold mine in October 2006 where an M=2.4 seismic event caused severe damage to a stope, fatally injuring several mine workers. Following the investigation of the event, it was noted that 25 minutes prior and close to the M=2.4 event a M=2.0 had occurred but caused no damage to the working places, consequently workers were not evacuated. It was suggested that the M=2.4 event might have been triggered by the quasi-static redistribution of stress following the M=2.0 event. The need for better understanding of changes in hazard following larger seismic events was recognised, as well as the formulation of guidelines regarding the evacuation of workers and re-entry times into working areas. This study assesses the hazard by analysing mine tremor aftershocks that succeed the seismic event.

During the course of the dissertation, the results obtained have been presented in local/international conferences and technical workshops such as the biannual South African Geophysical Association (SAGA) conference, Integrated Seismic Systems International (ISSI) conference, South African National Institute of Rock Engineering (SANIRE) conference, the Annual Africa Array workshop, the 3rd Annual Seismology workshop (Council for

Geoscience) and the General assembly of the International Association of Seismology and Physics of the Earth's Interior (IASPEI).

The results presented in the dissertation have also been presented in the following papers; Kgarume, T., and Spottiswoode, S., Density and rate of mine aftershocks and the implications for Seismic Hazard Assessment, *Africa Array workshop*, Jul. 2008, Kgarume, T., and Spottiswoode, S., Analysis of aftershock decay rates of mine seismic events, *South African Geophysical Association*, Sep. 2007 and Kgarume, T. E., Spottiswoode, S.M., and Durrheim, R. J., Statistical Properties of Mine Tremor Aftershocks, *Pure and Applied Geophysics*, 167, 2010, pp. 107–117, Kgarume T. E., Spottiswoode S. M., and Durrheim, R. J., Deterministic Properties of mine tremor aftershocks, *5th International Seminar on Deep and High Stress Mining*, Santiago Chile, October 2010 (In press). The author was also honoured with the best young presenter award at the 2009 SANIRE conference.

ABSTRACT

A methodology of assessing the seismic hazard associated with aftershocks is developed by performing statistical and deterministic analysis of seismic data from two South African deep-level gold mines. A method employing stacking of aftershocks is employed due to the small number of aftershocks succeeding each mainshock. Mine tremor aftershocks were found to obey statistical relations governing aftershocks (Gutenberg-Richter frequency-magnitude, Modified Omori law and the density law, with the exception of Båth's law) as natural earthquake aftershocks do. This analysis was used to approximate the time periods when the seismic hazard due to aftershocks has decreased to background levels. These time periods can be used to draw guidelines governing the re-entry periods to working areas following a larger seismic event. Deterministic analysis revealed that aftershock productivity is not strongly influenced by mining conditions (i.e. local stresses, strain rates, and the proximity to geological features such as faults and dykes).

ACKNOWLEDGEMENTS

The author wishes to thank the following people and organisations;

Prof. Ray Durrheim and Dr. Steve Spottiswoode for their encouragement and wonderful supervision,

- Dr Steve Spottiswoode for the development of the Omori code which was used to facilitate this work,
- Council for Scientific and Industrial Research (CSIR) for funding,
- Colleagues from the Seismology Research Group of the Centre for Mining Innovation (CSIR) for the valuable discussions and suggestion,
- Mine Health and Safety Council (MHSC),
- Mining companies for providing the datasets.

TABLE OF CONTENTS

DECLARATION II

PREFACE III

ABSTRACT VI

ACKNOWLEDGEMENTS VII

TABLE OF CONTENTS VIII

LIST OF FIGURES XI

LIST OF TABLES XIV

CHAPTER 1. INTRODUCTION 1

1.1 Motivation for study 2

1.2 Summary of dissertation 3

CHAPTER 2. SEISMIC EVENTS IN SOUTH AFRICAN GOLD MINES 5

2.1. Induced seismicity 5

2.2. Seismic monitoring in mines 6

2.3. Source mechanisms 7

2.4. Rock strength and deformation 8

2.5. Aftershock sequences 14

2.6. Statistical properties of aftershocks 16

2.6.1. Gutenberg-Richter frequency-magnitude relation 16

2.6.2. Båth's law 17

2.6.3 Modified Omori's Law 17

2.7. General geology of the Witwatersrand Basin 18

2.8. Carletonville Goldfields 19

CHAPTER 3. DATA AND METHODOLOGY 20

3.2. Influence of blasting on aftershocks 24

3.3. Datasets 26

CHAPTER 4. GUTENBERG-RICHTER RELATION 27

4.1. Introduction 27

4.2. Results and discussions 29

4.3. Conclusions 34

CHAPTER 5. BÅTH'S LAW 36

5.1. Introduction 36

5.2 Results and discussions 37

5.3 Conclusions 39

CHAPTER 6. MODIFIED OMORI LAW 41

6.1. Introduction 41

6.2. Results and discussions 42

6.2.1 Effect of bin size on aftershock event rate 42

6.2.2 Influence of blasting on aftershock event rate 44

6.2.3 Omori c-parameter 45

6.2.4 Aftershock event rate 47

6.3. Conclusions 56

CHAPTER 7. AFTERSHOCK DENSITY DECAY 58

7.1 Introduction 58

7.2 Results and discussions 59

7.3. Conclusions 63

CHAPTER 8. AFTERSHOCK PROBABILITY 64

8.1 Introduction 64

8.2 Results and discussions 65

8.3. Conclusions 69

CHAPTER 9. AFTERSHOCK PRODUCTIVITY 71

9.1. Introduction 71

9.2 Results and discussions 78

9.3. Conclusions 87

CHAPTER 10. CONCLUSIONS AND FURTHER RESEARCH 88

REFERENCES 90

LIST OF FIGURES

Figure 2.1: Simplified events mechanisms encountered in mining environments (section views). 7

Figure 2.2: Shear failure along a plane due to the applied stresses 8

Figure 2.3: Strength behaviour of a rock sample 10

Figure 2.4: Stress-strain behaviour of a rock sample. 11

Figure 2.5: The geology of the Witwatersrand basin. 18

Figure 3.1: Aftershock-mainshock sequences showing the typical small number of aftershocks following each mainshock. 20

Figure 3.2: Stacking of different mainshock-aftershock sequences. 21

Figure 3.3: A simplified flow chart for the program Omori. 22

Figure 3.4: Distribution of $M_L \geq 0.0$ aftershocks by hour of day within 1000 m of the mainshock epicentre. 25

Figure 4.1:Gutenburg-Richter frequency-magnitude relation of aftershock and background seismicity at the VCR mine. 30

Figure 4.2: Gutenburg-Richter frequency-magnitude relation of aftershock and background seismicity at the CLR mine. 31

Figure 5.1: Bath's law analysis of $M \geq 0.0$ aftershocks within 1000 m of and 2 hour following 163 $M \geq 2.0$ mainshocks (VCR mine). 38

Figure 5.2: Bath's law analysis of $M \geq 0.0$ aftershocks within 400 m of and 1 hour following 517 $M \geq 2.0$ mainshocks (CLR mine). 38

Figure 5.3: Increase of ΔM with increasing mainshock magnitude 39

Figure 6.1: Effect of number of events per bin on the event rate decay curve. 43

Figure 6.2: Estimation of the background rate. Long-term average determined by averaging over long-term seismicity (shaded area).....45

Figure 6.3: Time-magnitude distribution of aftershocks (CLR mine). 46

Figure 6.4: Time-magnitude distribution of aftershocks (VCR mine). 47

Figure 6.5: M ≥ 0.0 aftershock rate decay following mainshocks with threshold magnitudes M ≥ 1.0, M ≥ 2.0, and M ≥ 3.0. The lines representing p = 1 and the estimated background level are also shown. 49

Figure 6.6: M ≥ -0.5, M ≥ 0.0 and M ≥ 0.5 aftershock rate decay following mainshocks with magnitude M ≥ 1.0. The line representing the estimated background level is also shown. 49

Figure 6.7: M ≥ 0.0 aftershock rate decay within different radial distances from M ≥ 1.0 mainshocks. The line representing the estimated background level is also shown. 50

Figure 6.8: Event rate contour plots as a function of time and distance from 2.0 ≤ M ≤ 3.0 mainshocks (VCR mine). 51

Figure 6.9: Event rate contour plots as a function of time and distance from 3.0 ≤ M ≤ 4.0 mainshocks (VCR mine). 52

Figure 6.10: Event rate contour plots as a function of time and distance from 2.0 ≤ M ≤ 3.0 mainshocks (CLR mine). 52

Figure 6.11: Event rate contour plots as a function of time and distance from 3.0 ≤ M ≤ 4.0 mainshocks (CLR mine). 53

Figure 6.12: Determination of time periods where the event rate has decreased to background levels. 54

Figure 7.1: Aftershock density as a function of distance from the mainshock. 61

Figure 7.2: Aftershock density as a function of distance from the mainshock. 62

Figure 8.1: M ≥ 0.0 Aftershock probabilities for VCR mine within 1 day following, (a) 2.0 ≤ M ≤ 2.5 mainshocks and (b) 3.0 ≤ M ≤ 3.5 mainshocks…68

Figure 8.2: M ≥ 0.0 Aftershock probabilities for CLR mine within 1 day following, (a) 2.0 ≤ M ≤ 2.5 mainshocks and (b) 3.0 ≤ M ≤ 3 .5 mainshocks..68

Figure 9.1: Dependency of aftershock productivity on mean heat flow for 5 regions in Southern California.....72

Figure 9.2: Subsets defining three mining conditions. (A) Stress influence (red and blue colour represent high and low stress conditions respectively), (B) Strain rate influence (blue colour represent active mining) and (C) Geological discontinuity influence.....74

Figure 9.3: Division of mainshocks into two populations to study the influence of geological discontinuities on aftershock productivity.....76

Figure 9.4: M ≥ 0.0 aftershock decay rate following 2.0 ≤ M ≤ 3.0 mainshocks. 79

Figure 9.5: Aftershock productivity within 1000 m and 1 day following M ≥ 2.0 mainshocks.....80

Figure 9.6: Aftershock productivity dependency on stress environments.....81

Figure 9.7: Aftershock productivity dependency on geological discontinuities. 82

Figure 9.8: Aftershock productivity dependency on strain environments. 82

LIST OF TABLES

Table 2.1: Elastic constants and strength properties of rock types encountered in the gold mines. 13

Table 3.1: Summary of data catalogues used in the analysis. 26

Table 4.1: Least squares estimates of the *a*- and *b*-parameters of the Gutenburg-Richter frequency-magnitude relation for the VCR and CLR mines. 32

Table 4.2: Maximum likelihood estimate of the *b*-parameter of the Gutenburg-Richter frequency-magnitude relation (VCR). 33

Table 4.3: Maximum likelihood estimate of the *b*-parameter of the Gutenburg-Richter frequency-magnitude relation (CLR). 33

Table 6.1: Time periods required for the aftershock event rate to reach 10× and 3× the background rate. 55

Table 8.1: Summary of the parameters used in the probability models (VCR mine). 66

Table 8.2: Summary of the parameters used in the probability model (CLR mine). 67

Table 9.1: Statistical comparison of aftershock productivity for contrasting mining environments. 84

Table 9.2 : Proportion of aftershocks (VCR mine) 86

Table 9.3: Proportion of aftershocks (CLR mine) 86

CHAPTER 1. INTRODUCTION

Seismic events in mines pose a risk to underground personnel, may damage underground infrastructure and lead to loss of production. Seismology in mines is used to asses seismic hazard associated with deep level mining, and has proven over the years to be an important tool in understanding the mechanisms of these mining related events. Seismic hazard assessments in mines are carried out routinely, specifically to assess likelihood of a mainshock occurring. Although substantial work has been carried out in developing methodologies for these assessments, less focus has been placed in developing such methodologies for assessing any change in hazard following the mainshock.

In this work focus is placed on developing a methodology for assessing the seismic hazard associated with aftershocks succeeding the initiating mainshock. The method is developed in two phases. The first phase assesses the hazard by considering the statistical properties of aftershocks. In the second phase, a deterministic approached is followed to assess the dependency of aftershocks on mining conditions.

1.1 Motivation for study

The main objective of this project is to develop a methodology to assess the seismic hazard posed by aftershocks following larger seismic events ($M \geq 2.0$). The study aims to identify distances and time periods, following the main events, where the hazard posed by aftershocks has decreased to background levels. In addition, the project will also study the physical processes governing the behaviour of mine tremor aftershocks. Two main approaches were used to assess the hazard:

- Statistical data analysis, where statistical properties of aftershocks were studied by analyzing the properties of stacked aftershock data.
- Deterministic data analysis, where the hazard was evaluated by considering aftershock behaviour (productivity changes) in different mining conditions (e.g. highly-stressed mining faces versus relatively unstressed mining faces).

This work is unusual in that it estimates the seismic hazard posed by aftershocks, while most studies only consider the seismic hazard posed by main events.

1.2 Summary of dissertation

Chapter 1 gives a general introduction to the dissertation and the motivation for the study. In chapter 2, a more detailed discussion of the seismic events encountered in the South African gold mines is given. The discussions include seismic monitoring in mines, seismic source mechanisms and rock strength and deformation. Section 2.5 is of particular relevance to this dissertation, as it discusses aftershock sequences, their triggering mechanisms and most importantly, their statistical properties. Sections 2.7 and 2.8 provide a brief review of the geology of the Witwatersrand basin and the Carletonville goldfields (source area of the datasets).

Chapter 3 discusses the data, methodology and procedures employed in the analysis. The procedure utilised by the custom-written computer program, OMORI, and the method used to account for the influence of daily blasting on aftershocks are discussed. Chapter 4 to Chapter 9, which make up the body of the dissertation, describe the analysis. The statistical approach is described in Chapters 4 to 8, and the deterministic data analysis in Chapter 9.

Chapters 4, 5 and 6 discuss, in more detail, the Gutenberg-Richter relation, Båth's law and the Modified Omori law applied to mine tremor aftershocks. These chapters are essential particularly for the hazard assessment following the mainshock. Chapter 7 discusses aftershock density decay with distance

from the mainshock. The rate of aftershock decay is an indicator of the stress transfer mechanisms and is analysed in order to understand the triggering mechanism of mine tremor aftershocks. Chapter 8 discusses aftershock probability by combining all the statistical properties of aftershocks (with the exception of Båth's law) into a rate equation that gives the probability of one or more aftershocks occurring in the magnitude range $M_1 \leq M \leq M_2$, time range $t_1 \leq t \leq t_2$ and distance range $r_1 \leq r \leq r_2$ from the mainshock of magnitude M_{main}. Chapter 9 investigates the dependency of aftershock productivity on mining conditions in an attempt to understand the physical processes governing the aftershock generation processes. Conclusions and considerations for further research are given in Chapter 10, which concludes the dissertation.

CHAPTER 2. SEISMIC EVENTS IN SOUTH AFRICAN GOLD MINES

2.1. Induced seismicity

Seismicity in mines is a consequence of the rockmass response to stresses induced by mining, which result in elastic and inelastic deformations of the rock surrounding an excavation. A seismic event results from the sudden release of the accumulated elastic strain energy (Jager and Ryder, 1999, pg. 287) and is defined as a sudden inelastic deformation within a given volume of rock that radiates detectable seismic waves (Mendecki, 1997, pg. 178). To indicate the triggering effect of human activity, this type of seismic activity is usually called induced seismicity (Gibowicz and Kijko, 1994, pg. 1) and it is also encountered in other engineering operations such as amongst others, the filling of reservoirs, surface quarrying and the injection and removal of fluids (e.g. hydrocarbons) from the subsurface.

Although a systematic difference between mine events and natural earthquakes has not been found (Gibowicz and Kijko, 1994, preface), their driving forces are different. Long-wavelength stresses associated with the relative motions of tectonic plates provide the driving forces for natural earthquakes, while mine events are primarily driven by the mining and occur in regions where stress changes due to mining are greatest (McGarr,

Spottiswoode and Gay, 1975). In terms of similarity, Spottiswoode and McGarr (1975) found that mine events and earthquakes are similar with regards to stress drop, the relationship between moment and magnitude, and the relationship between size and magnitude. Their occurrence appears to be controlled by rock strength and the change in the stress field from virgin state (McGarr, Spottiswoode and Gay, 1975).

2.2. Seismic monitoring in mines

Routine seismic monitoring was introduced in underground mines for two main reasons: Immediate location of seismic events for guidance in rescue operations, and prediction of large rock mass instability (Mendecki, 1997, preface). Detection and analysis of seismicity can also provide useful information for the planning and control of mining operations (Ryder and Jager, 2002, pg 193).

Seismology has also proven to be an important tool in understanding the mechanisms of seismic events. Jager and Ryder (1999, pg. 24) summarised three conditions which should be met for the initiation of a seismic event:

- A zone of overstressed rock must firstly exist in a state of unstable equilibrium,
- A sufficient change in stress must occur in order to trigger the event, and

- The failing structure must undergo a significant and substantial rapid stress drop.

2.3. Source mechanisms

Two practical source mechanisms have been identified in mines, namely the crush-type and shear-type mechanisms (Figure 2.1).

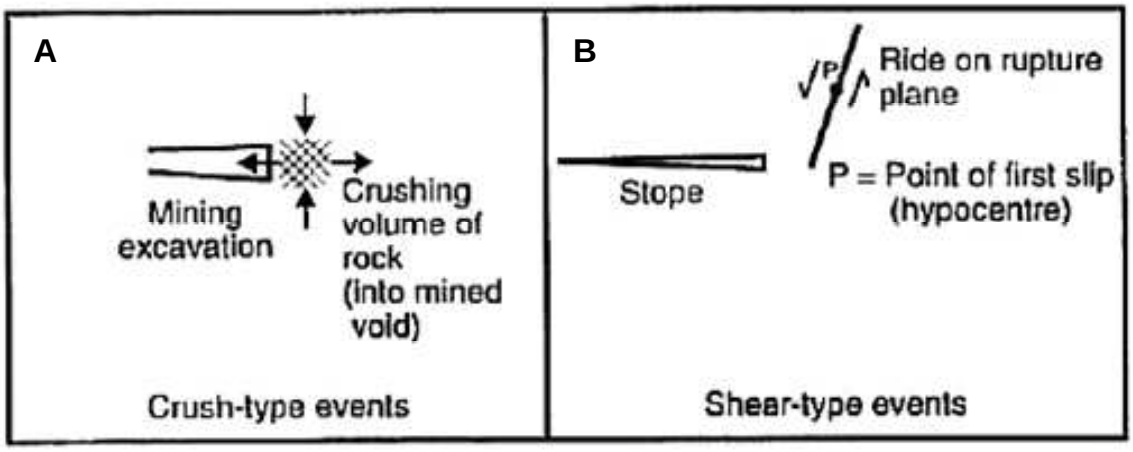

Figure 2.1: Simplified events mechanisms encountered in mining environments (section views).

(From Jager and Ryder, 1999, pg. 24)

Crush-type events, which exhibit a high degree of volumetric closure, tend to locate close to reef and to mining faces, and account for many small magnitude events ($M_L < 2$). Shear-type events, which account for most of the larger events ($M_L > 2$), tend to occur on planes of weaknesses such as faults, joints and dykes contacts (Jager and Ryder, 1999, pg. 24).

Understanding of these mechanisms and conditions required for their initiation requires an understanding of factors governing rock behaviour, such as rock stresses, rock strength and friction properties.

2.4. Rock strength and deformation

The most used criterion of failure is the Coulomb failure criterion. The criterion assumes that failure in rock occurs along a plane in the rock due to the shear stress acting along that plane (Figure 2.2).

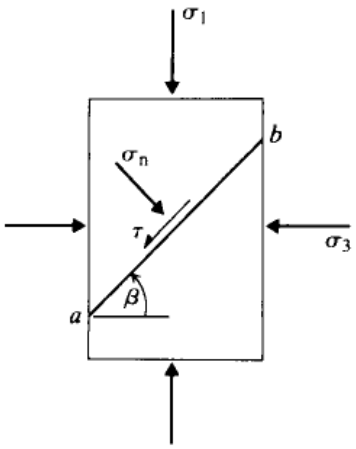

Figure 2.2: Shear failure along a plane due to the applied stresses.

(From Brady and Brown, 2004, pg. 105)

A rock mass transected by a weak plane (joint, faults or a dyke) will undergo slip along the plane if the plane is subjected to sufficiently high levels of shear stresses. The amount of slip and the severity of the seismic event resulting

from such a slip are dependent on the shear-strength properties of the plane (Ryder and Jager, 2002, pg. 225).

The Coulomb failure criterion is given by the equation;

$$|\tau| = c + \mu\sigma_n \tag{2.1}$$

where *c* is the cohesion, μ is the coefficient of internal friction and σ_n is the normal stress acting along the plane. The sign of the shear stress indicates the slip direction after failure. In earthquake seismology, the criterion has been used to study the distribution of aftershocks around a mainshock (e.g. Stein, 1999, Ganas et. al., 2008) and earthquake-induced static stress triggering on neighbouring faults in the vicinity of the mainshock (e.g. Pollitz et. al., 2002).

Rock strength and deformation characteristics are usually determined from laboratory experiments performed on small rock samples under uniaxial (confining stress σ_3=0) and triaxial conditions (confining stress σ_3>0). The strength behaviour of a rock is described by the Mohr-Coulomb failure criterion. The criterion (equation 2.2) is represented by a linear relationship in the σ_1: σ_3 plane where σ_1 and σ_3 are the principal stresses acting on the sample.

$$\sigma_1 = \sigma_c + \beta\sigma_3 \tag{2.2}$$

where σ_c is the Uniaxial Compressive Strength (UCS) and β is the strengthening parameter with $3 \leq \beta \leq 5$ for stronger rock types (Jager and

Ryder 1999, pg.14). Figure 2.3 summarises the strength behaviour of a rock sample.

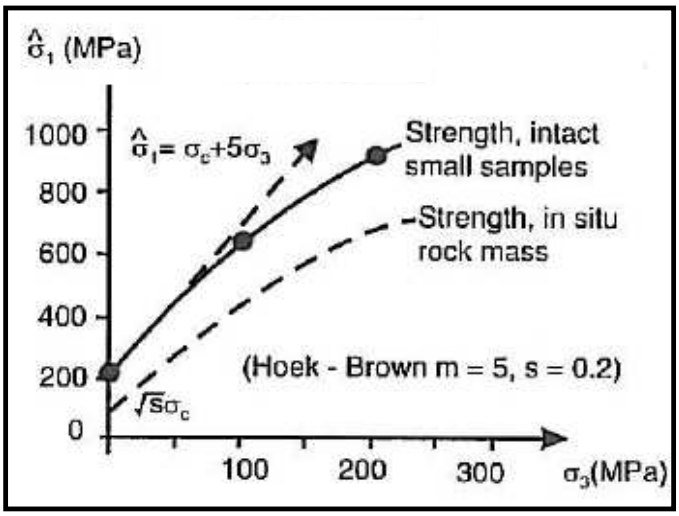

Figure 2.3: Strength behaviour of a rock sample.

(From Jager and Ryder, 1999, pg. 13).

In practice, however, it is found that the strength characteristics of intact rock samples display a downward curvature and the strength of the in situ rockmass can be less than that of small intact samples (Figure 2.3). This is due to geological weaknesses that usually transect the rockmass.

The empirical Hoek-Brown Criterion (equation 2.3) was introduced to cater for these effects that the Mohr-Coulomb criterion does not address.

$$\sigma_1 = \sigma_3 + \sqrt{s\sigma_c^2 + m\sigma_c\sigma_3} \qquad (2.3)$$

where s (typically 0.01 ≤ s ≤ 0.6) characterises the rock mass condition and m (typically 0.05 ≤ m ≤ 5) characterises the curvature of the curve (Jager and Ryder 1999, pg.14). Estimates of s and m can be determined from rock mass classification surveys. Brady and Brown (2005) list three important parameters that describe the behaviour of rock:

- Constants relating stresses and strains in the elastic range,
- Stress levels at which yield, fracturing and slip occurs, and
- Post-peak stress-strain behaviour of the fractured rock.

The general behaviour of a rock sample as a function of applied stress and strain is illustrated in Figure 2.4.

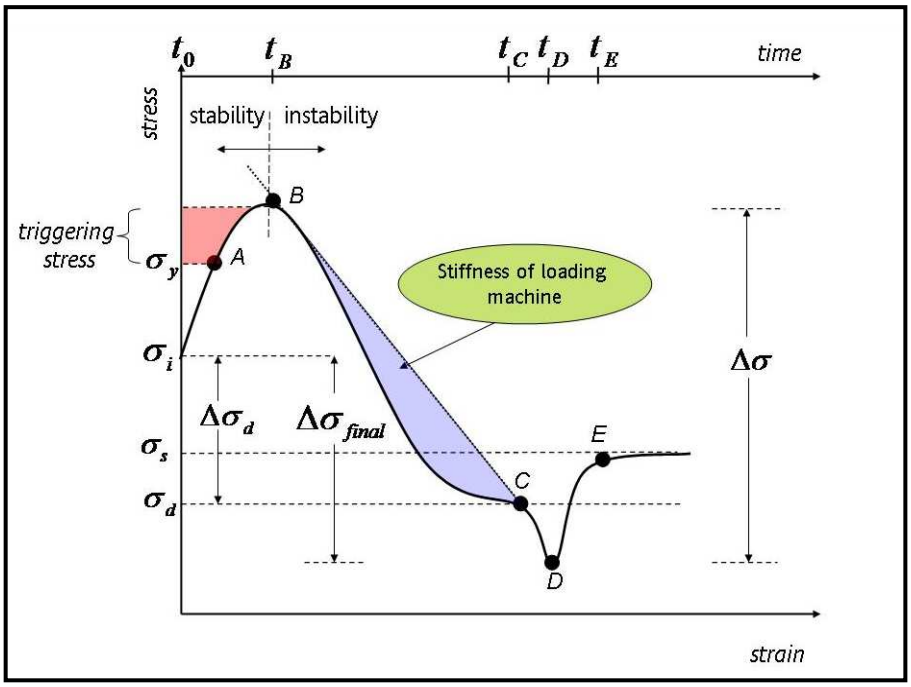

Figure 2.4: Stress-strain behaviour of a rock sample.

A rock specimen subjected to an applied stress F/A (F is the force and A is the area) will undergo elastic deformation until a yield stress is reached. Failure (which refers to the reduction of the specimen's load carrying capacity due to crack initiation and growth) occurs when the stress exceeds the static peak strength resulting in slip initiation. At this point irreversible and permanent deformation continues and a further increase in applied stress brings the specimen to its peak strength (point B in figure 2.4). This additional stress needed to bring the specimen to its peak strength is termed the triggering stress (In uniaxial conditions the peak-strength is defined as the Uniaxial Compressive Strength).

Consider a point P (on the plane of slip) with the applied stress at its initial value σ_i at time t_0 being approached by rupture (figure 2.4). As the rupture approaches, the stress at P rises due to dynamic stress concentration ahead of the propagating crack. When the rupture reaches P and the dynamic stresses reach σ_y (point A), slip is initiated and over some critical slip distance *L*, frictional resistance changes from a static coefficient μ_s to a lower dynamic coefficient μ_d. Assuming that the dynamic friction stress σ_d remains constant during slip, the residual strength of the specimen (point C) is reached at time t_B after considerable post-peak deformation and stress drop $\Delta\sigma$. The slope of the line joining the peak strength (point B) and the residual strength (point C) gives the stiffness of the loading machine (Brady and Brown, 2005, pg. 98). Healing (cessation of slip) initiates following the termination of rupture

at time t_C (point C). After healing, the stress increases further due to dynamic overshoot of the slip so that the final stress drop is greater than the dynamic stress drop (point D) (Scholz, 1990, pg. 175, Madariaga, 1976). After the overshoot the static friction increases further to a value above the dynamic friction (point E). This behaviour where the static friction stress σ_s is greater than the dynamic friction stress is known as velocity weakening (Scholz, 1990, pg. 75, Madariaga, 1976) thus the sample can sustain an increase in stress without failing. This behaviour is described by the rate- and state-dependent friction law. Examples of elastic constants and strength properties of rock types encountered in the gold mines are given in Table 2.1.

Table 2.1: Elastic constants and strength properties of rock types encountered in the gold mines.

E – Young's modulus, *v* – Poisson's ratio, UCS – uniaxial compressive strength.

Rock type	**E (GPa)**	ν	**UCS (GPa)**
Quartzite	65 – 75	0.20 – 0.25	160 – 280
Argillaceous Quartzite	50 – 70	0.18 – 0.22	130 – 200
Lava	60 – 100	0.25 – 0.30	100 – 500

2.5. Aftershock sequences

Aftershocks often occur following the main event. They can be thought of as a form of brittle response of the crust to stresses loaded by the mainshock. Scholz (1990) explains aftershocks as a process that relaxes stresses produced by the mainshock rupture. Aftershock sequences begin immediately after the main event and are concentrated in the rupture area and its surroundings. This distinctive behaviour of aftershocks has been used to estimate the source dimensions of the mainshock (Gibowicz, 1973). Having said that, however, some aftershocks have been found to occur at remote distances away from the mainshock (Freed, 2005; Hill, 2007). Such interaction between a mainshock and its aftershocks has been studied and currently three modes of triggering are accepted: static stress transfer, quasi-static stress transfer, and dynamic stress transfer, with the stress amplitudes falling with distance as r^{-3}, r^{-2} and $r^{-1.5}$, respectively (Hill, 2007).

Triggering of aftershocks by static and quasi-static stress transfer is well explained by the Coulomb failure criterion. The triggering is caused by permanent stress changes produced by the mainshock in the vicinity of a fault, bringing other regions closer to their Coulomb failure threshold. Static stress transfer occurs instantaneously, and decays rapidly with distance (as r^{-3}), hence its triggering potential is limited to one or two source dimensions. The static model has been successfully used to explain the distribution of aftershocks around the region of the mainshock (Stein, 1999;

Stein and Lisowski, 1983), but fail to explain the triggering of events at remote distances.

Quasi-static stress transfer, which is due to viscous relaxation of the crust following an earthquake (Pollitz and Sacks, 2002), decays more slowly with distance (as r^{-2}) and its triggering potential extends to relatively greater distances. Because of the low propagation speeds of viscoelastic deformation, it can result in delayed triggering (Hill, 2007). Although this is an unlikely triggering mechanism in mines, as it generally occurs in the lower crust and upper mantle, viscoelastic modelling of the rock mass has been successfully used in the deep level tabular excavation to simulate the observed stope closures in the VCR and Vaal Reef (Malan, 1995). Malan (1999) also successfully used Elasto-viscoplastic modelling to simulate the time-dependent closure behaviour at these reefs, with the time-dependent closure data possibly indicating the stress conditions in the fracture zone ahead of the face.

Dynamic stresses propagating as seismic waves are, however, capable of triggering earthquakes at remote distances as their decay with distance is much slower. Dynamic stresses are transient and oscillatory, altering stresses further from or closer to the Coulomb failure of the fault. They do not result in permanent stress changes, but may cause changes in the rock mass that bring faults closer to their Coulomb failure, and could thus explaining remote triggering. Felzer and Brodsky (2006) found that the density of aftershocks

falls off with distance from the mainshock as $r^{-1.3}$, supporting the dynamic triggering model.

2.6. Statistical properties of aftershocks

Earthquake aftershocks have been found to satisfy three scaling relations. The important statistical relations are discussed below.

2.6.1. Gutenberg-Richter frequency-magnitude relation

This law approximates the frequency-magnitude statistics of earthquakes very well. It relates the number of events to their magnitude and was proposed by Gutenberg and Richter (1954).

$$\log N(\geq M) = a - bM \tag{2.4}$$

N (≥ *M*) is the number of events with magnitude greater or equal to *M* in a given time interval, *b* is a constant generally in the range $0.8 < b < 1.2$ (Frolich and Davis, 1993) and of importance in earthquake hazard analysis (Guttorp, 1987), and *a* is a constant which measures the regional level of seismicity and is given by the logarithm of the number of events with magnitude greater or equal to zero.

2.6.2. Båth's law

Båth's law gives the relationship between a mainshock and its largest aftershock and states that their magnitude difference (*ΔM*) is a constant independent of the mainshock magnitude.

$$\Delta M = M_{ms} - M_{as}^{\max} \approx CONSTANT \tag{2.5}$$

For earthquakes, ΔM typically has a value of about 1.2 (Båth, 1965, Shcherbakov et al., 2006).

2.6.3 Modified Omori's Law

This law describes the temporal decay of aftershock activity.

$$n(t) = \frac{K}{(t+c)^p} \tag{2.6}$$

t is the time after the mainshock, *n(t)* is the number of events occurring at time *t*, *K* and *c* are parameters and *p* is a rate constant of aftershock decay (Nanjo et al., 1998) and has a value close to 1.

2.7. General geology of the Witwatersrand Basin

The Witwatersrand basin (Figure 2.5) hosts the world's largest deposits of gold and uranium. During deposition, a large inland sea drained an auriferous terrain of Basement granites and greenstone belts. It is currently accepted that the Witwatersrand basin formed in a compressive foreland setting, possibly related to the collision of the Zimbabwe and Kaapvaal Cratons (McCarthy, 2006, pg. 179).

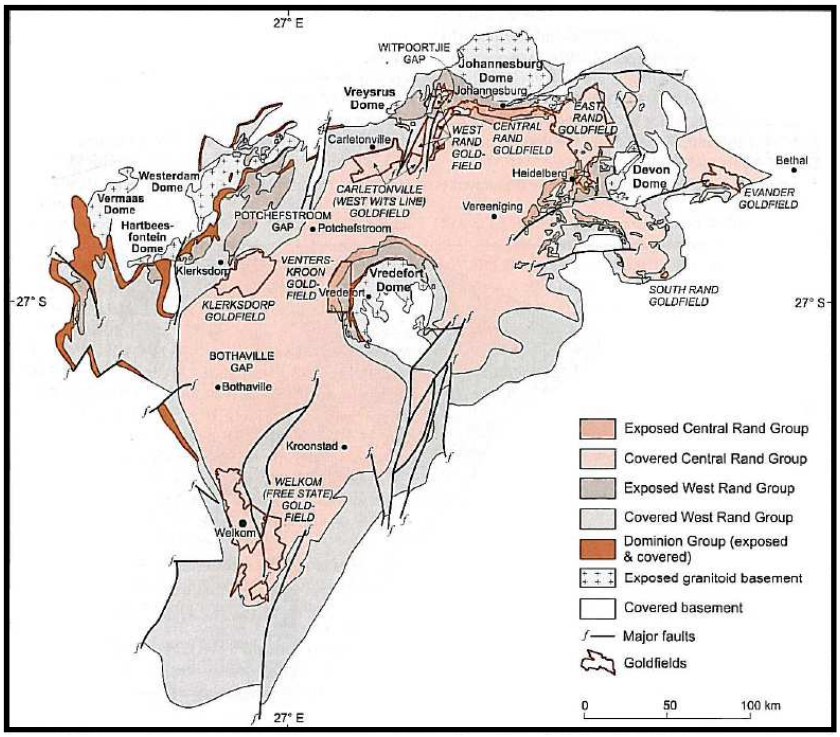

Figure 2.5: The geology of the Witwatersrand basin.

(From McCarthy, 2006, pg. 157)

The basin has been dated to the Archean between 3074 million years and 2714 million years (Robb and Robb, 1998, pg. 299).

2.8. Carletonville Goldfields

This study was undertaken on mines of the Carletonville goldfield (also known as the West Wits Line). The goldfield is situated between the Potchefstroom gap in the west and the West Rand fault (Figure 2.5). The most important gold-bearing reefs being mined are the Carbon Leader Reef (CLR) at the base of the Main Formation and the Ventersdorp Contact Reef (VCR) at the base of the Ventersdorp Supergroup.

The Ventersdorp Contact Reef occurs in the northwest and western margins of the basin in the West Rand, Klerksdorp and Carletonville goldfields. The VCR lies unconformably on the Witwatersrand sediments and is considered to be the basal reef of the Ventersdorp Supergroup (Jager and Ryder, 1999, pg. 29). The reef is separated from its lava hanging-wall by a band of quartzite up to 1 metre thick. The footwall is composed of a strong argillaceous quartzite. Hazardous hangingwall conditions are often encountered due to the bedding-parallel faulting that occurs in the quartzite and extends into the lava hangingwall.

The Carbon Leader Reef (CLR) is a narrow, carbon-rich conglomerate band, rarely exceeding 10 cm in thickness in the Carletonville area (Robb and Robb, 1998). The hanging-wall consists of a pebbly grit, invariably overlain by a shale band known as the Green Bar.

CHAPTER 3. DATA AND METHODOLOGY

Large seismic events in deep-level gold mines are often followed by an increased rate of seismicity. The number of aftershocks following any single mainshock is usually quite small, typically fewer than five aftershocks of M_L>0 for each M_L>2.5 mainshock, which is too few for reliable statistical analysis such as frequency-magnitude relationship of aftershock sequences (Figure 3.1).

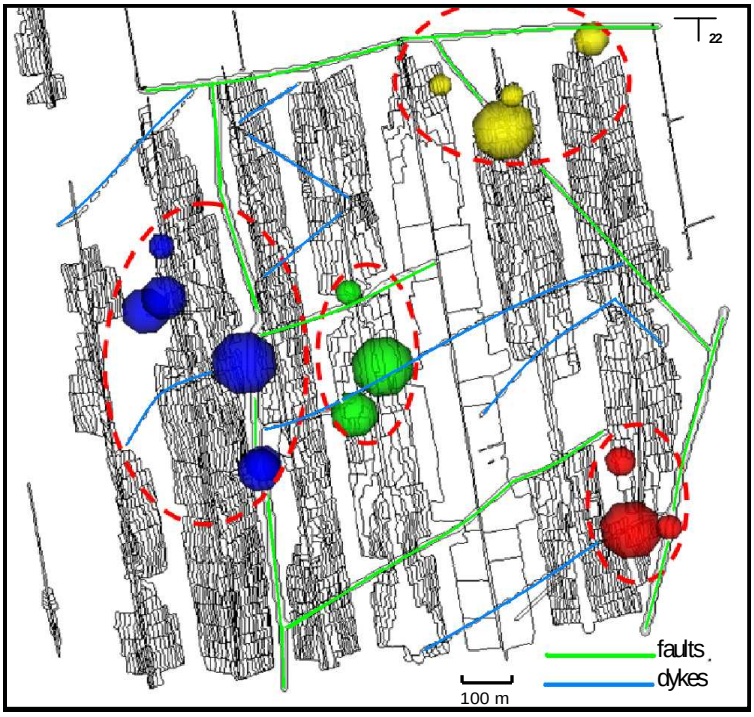

Figure 3.1: Aftershock-mainshock sequences showing the typical small number of aftershocks following each mainshock.

Large and smaller circles represent mainshocks and aftershocks respectively. The colours indicate the different days of occurrence of the clusters.

To overcome this limitation, a method of data stacking was used where mainshock-aftershock sequences are stacked at the origin in time and space (Figure 3.2). This allows for the study of aftershocks sequences with time and distance away from the mainshock epicentre.

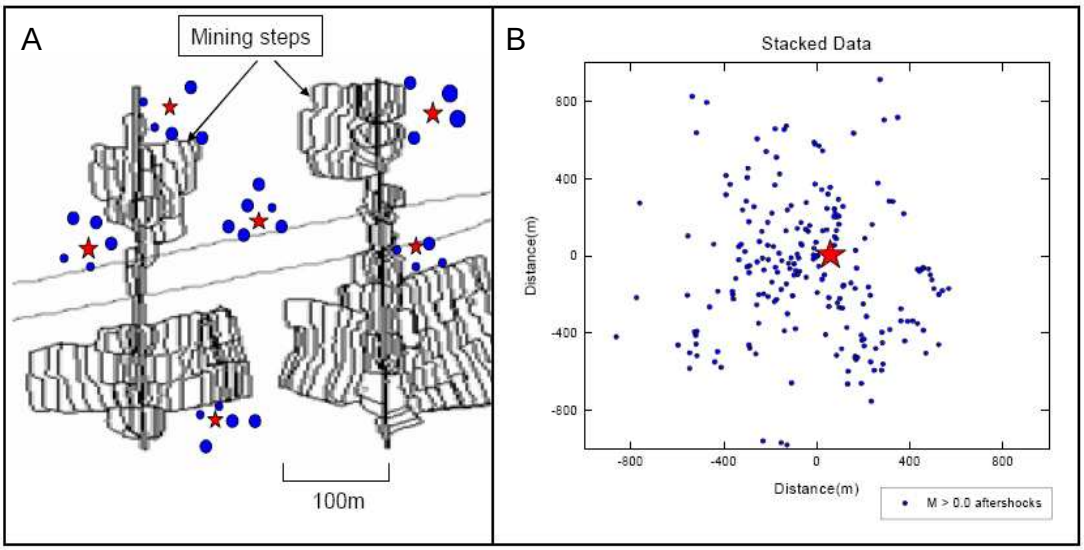

Figure 3.2: Stacking of different mainshock-aftershock sequences.

(A) Cartoon showing mainshocks-aftershock clusters overlaid on a mine plan (red stars and blue circles represent mainshock and aftershocks respectively). Monthly positions of stope advance (mining steps) are represented by rectangular bands.

(B) M_L > 0.0 aftershocks stacked at the origin in space.

The stacking procedure was facilitated by a custom-written program Omori (software written by Spottiswoode, 2002, adapted from work by Spottiswoode, 2000) that stacks mainshocks temporally and spatially, and reports on the

time and distance behaviour of aftershocks following a mainshock. A simplified flow chart of the program is shown in Figure 3.3.

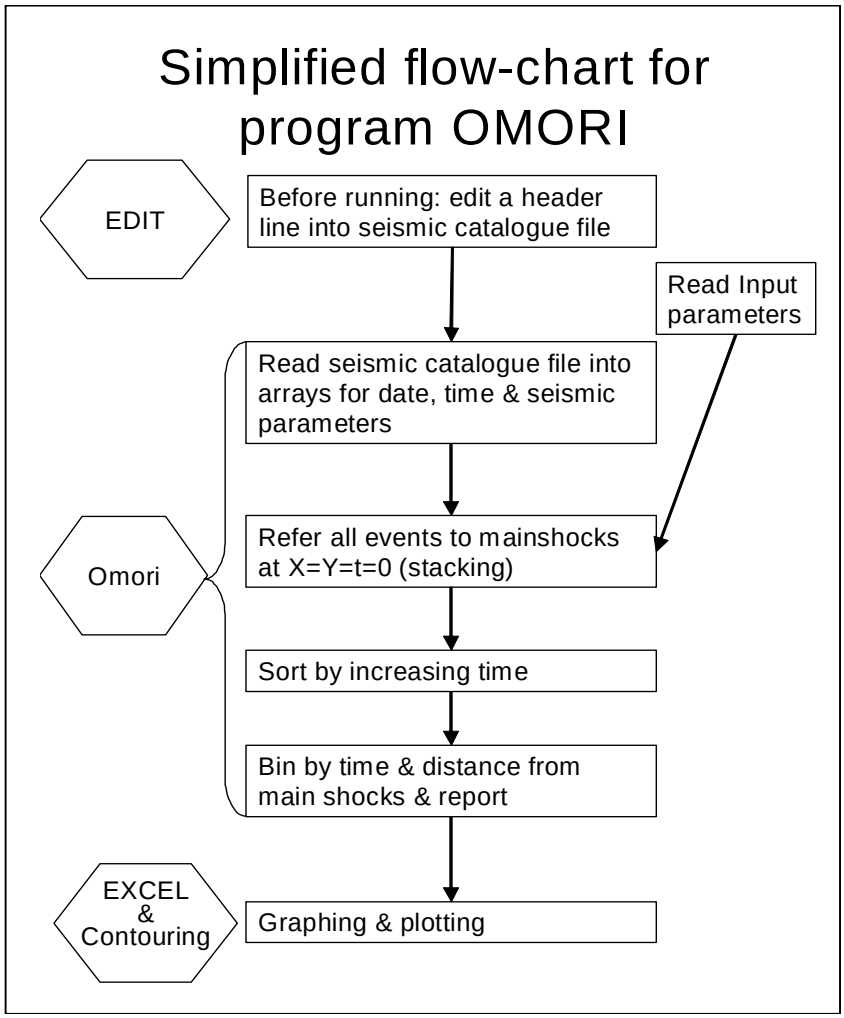

Figure 3.3: A simplified flow chart for the program Omori.

(From Spottiswoode, 2000).

Following the editing step, the program refers all mainshocks to the origin in space and time. Input parameters for the stacking procedure are:

- Upper and lower threshold magnitudes for mainshock and aftershocks,
- Maximum time for listing of aftershocks following the mainshock,
- Maximum distance for listing of aftershocks from mainshock,
- Bin size (number of events within a bin),
- Range of distance for focus to mining face, and
- Range of face Energy Release Rate (explained in detail in later chapter).

In the search through the catalogue, a mainshock is defined as an event with magnitude less than the upper threshold magnitude and greater than the lower threshold magnitude. Aftershocks are events within the maximum time and distance limit from the mainshock with magnitude less than the mainshock magnitude.

Aftershocks are then sorted by increasing time from the mainshocks, binned by time and distance away from the mainshocks, and reported. Another important factor considered in the stacking procedure is the increasing seismicity following blasting. It should be noted that blasting-relating events (events occurring during blasting time) were not considered in this study as their influence serves to contaminate the seismic activity of interest. Blasting-related events were rejected from the analysis using the method developed by Richardson and Jordan (2002) and refined by Spottiswoode and Linzer (2006). Their influence on aftershocks is discussed next.

3.2. Influence of blasting on aftershocks

It is important to consider the effects of blasting on seismicity so that their effect can be corrected to achieve accurate analysis. Two kinds of blasting occur in underground mines; development blasting (e.g. for the development of tunnels), and production blasting (e.g. for the advancement of the stope faces). The blasting periods can be clearly identified by observing the distribution of the number of aftershocks by hour of day in a 24 hour period.

Figure 3.4 illustrates the effect of blasting on the number of mine tremor aftershocks, with a significant increase at the onset of blasting at 18h00 at VCR (mine1) and at 12h00 at CLR (mine 2). Bins are referenced to the start of each hour, e.g. bin 1 contains the number of events between 00:00:00 and 01:00:00.

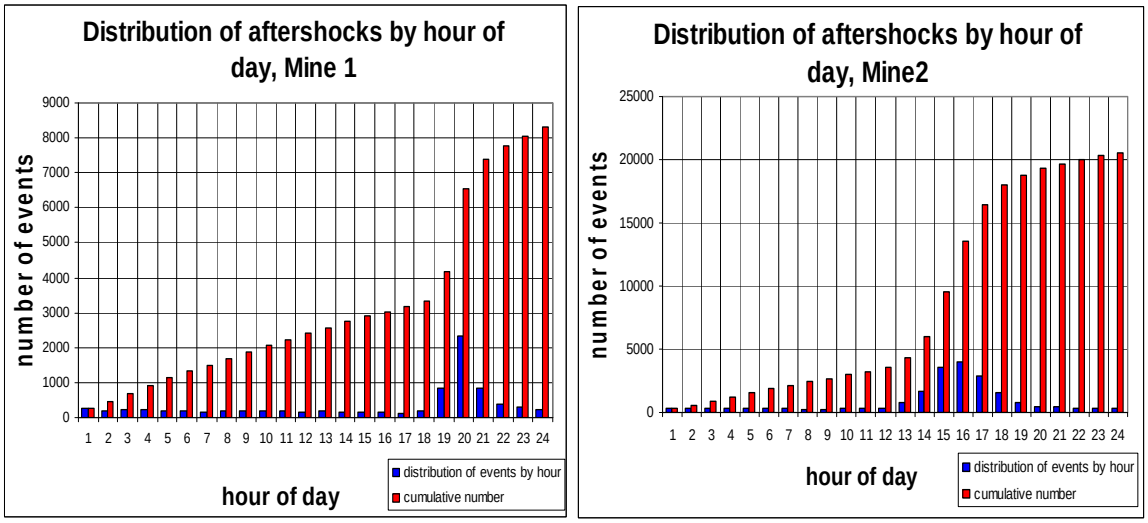

Figure 3.4: Distribution of $M_L \geq 0.0$ aftershocks by hour of day within 1000 m of the mainshock epicentre.

The broader distribution at mine 2 is probably due to different blasting techniques. It can be seen from the plotted cumulative number of events that blasting has the effect of doubling the number of events following its onset. Mainshocks occurring during the identified blasting periods or in the period 4 hours prior to the onset of blasting are then excluded from the analysis to avoid inclusion of the undesired seismicity triggered by normal production blasting from aftershock sequences.

3.3. Datasets

Seismic datasets from two deep-level gold mines situated in the Carletonville mining district, where mining is at depths of about 3,5 km, were provided for the analysis. Although triaxial geophones (typically 4.5 Hz) are employed to give better location accuracy and parameter estimates, seismic stations are mostly located close to the reef plane. This tends to increase the location error in the z-component, although decreasing it in the reef plane.

Although there are different measures of the magnitude of an event, such as body wave magnitude M_b or surface wave magnitude M_s, South African mines tend to favour the more widely used local magnitude, M_L which was introduced by Richter (1935) and adjusted accordingly for the mines. Table 3.1 gives a summary of the two catalogues used in the analysis.

Table 3.1: Summary of data catalogues used in the analysis.

Reef mined	**VCR**	**CLR**
Start time	2002/08/01	1998/01/02
Total number of events recorded	10196	20611

CHAPTER 4. GUTENBERG-RICHTER RELATION

4.1. Introduction

The Gutenberg-Richter relation (equation 2.4) successfully approximates the frequency-magnitude statistics of earthquakes, except at high magnitudes where it often overestimates the likelihood of the occurrence of large events (Gibowicz, 1994, pg. 302). The b-value is usually determined by the method of least squares (Shcherbakov et. al, 2005, 2006), where *b* is found from the least squares fit of a straight line to equation (2.4) and given by the slope of the regression line.

A more accurate estimate of the b-value was suggested by Aki (1965) using the method of maximum likelihood where seismic events are assumed to be independent, identically distributed random variables with probability density function $f(M,\beta)$ expressed by;

$$f(M,\beta)=\beta e^{-\beta(M-M_{\min})}, M_{\min}\le M \tag{4.1}$$

The parameter β is given by

$$\beta = b/\log_{10} e \tag{4.2}$$

and the best statistical estimator of *b* is the maximum likelihood estimator (MLE) of β given by

$$\hat{\beta} = \frac{1}{< M > - M_{\min}} \tag{4.3}$$

where the sample mean $< M >= \sum_{i=1}^{N} M_i / N$ and $M_{\min}$ is the minimum magnitude of the events. Aki (1965) showed that the 95 % confidence limits of $\hat{\beta}$ are given by

$$\frac{\left(1 - d_\varepsilon / \sqrt{N}\right)}{< M > - M_{\min}} \leq \hat{\beta} \leq \frac{\left(1 + d_\varepsilon / \sqrt{N}\right)}{< M > - M_{\min}} \tag{4.4}$$

where ε=95% is the confidence interval and d_ε=1.96 for the ε confidence interval. The *b*-value is then given by

$$b = \frac{\log_{10} e}{< M > - M_{\min}} \tag{4.5}$$

and the standard deviation of b is given by $\hat{\sigma}_\beta \log_{10} e$, where $\hat{\sigma}_\beta$ is the standard deviation of $\hat{\beta}$ which is approximately normally distributed about its mean value equal to equation 4.2 (Gibowicz, 1994, pg. 304).

The Gutenberg-Richter relation, which implies a fractal relationship between the number of earthquakes and the size of the rupture area (Turcotte, 1997), has also been found to hold for mine seismic events. The constant *b* or the “b-value” was suggested by Aki (1981) to be related to the fractal dimension *D* of the source region by equation 4.6 below.

$$D = 2b \tag{4.6}$$

A b-value of 0.5, which corresponds to *D* = 1, would be related to seismic events distributed along a one-dimensional linear source. For a b-value of 1.0, *D* = 2, and is related to seismic events distributed within a two-dimensional planar source. A b-value of 1.5, corresponding to *D* = 3, suggests volumetrically distributed sources (Legge and Spottiswoode, 1987).

If b = 0.5, *D* = 1 and planar seismic source zones with L(length) » W(width) are indicated. This situation arises when there is extensive mining parallel to a fault or dyke. The excess shear stress lobes produced by the excavations extend for hundreds of metres in the strike direction of the fault or dyke (L), but only for tens of metres in the dip-direction (W). If b = 1, *D* = 2 and planar seismic source zones with L and W are indicated. This situation arises where the source dimension parallel to the mining face (L) is limited to tens of metres by the leads and lags between adjacent panels. If b = 1.5, *D* = 3 and volumetrically distributed sources are indicated with L and W and S, where S is the shear-zone spacing. In practical terms, this means that the volume of rock contributing to each event is further limited by the presence of shear zones.

4.2. Results and discussions

Analysis of the Gutenberg-Richter frequency-magnitude was performed on $M_L \geq 0.0$ aftershocks following $M_L \geq 2.0$ mainshocks from the two mines. The

b-values of the data were estimated using the least squares and maximum likelihood methods. Figure 4.1 and Figure 4.2 show the Gutenberg-Richter frequency-magnitude of events that occurred within 1 hour and 1000 m of $M_L \geq 2.0$ mainshocks. These events are temporally close to the mainshock and thus considered as aftershocks. Also plotted are events occurring more than 6 hours following $M_L \geq 2.0$ mainshocks and considered to be background events.

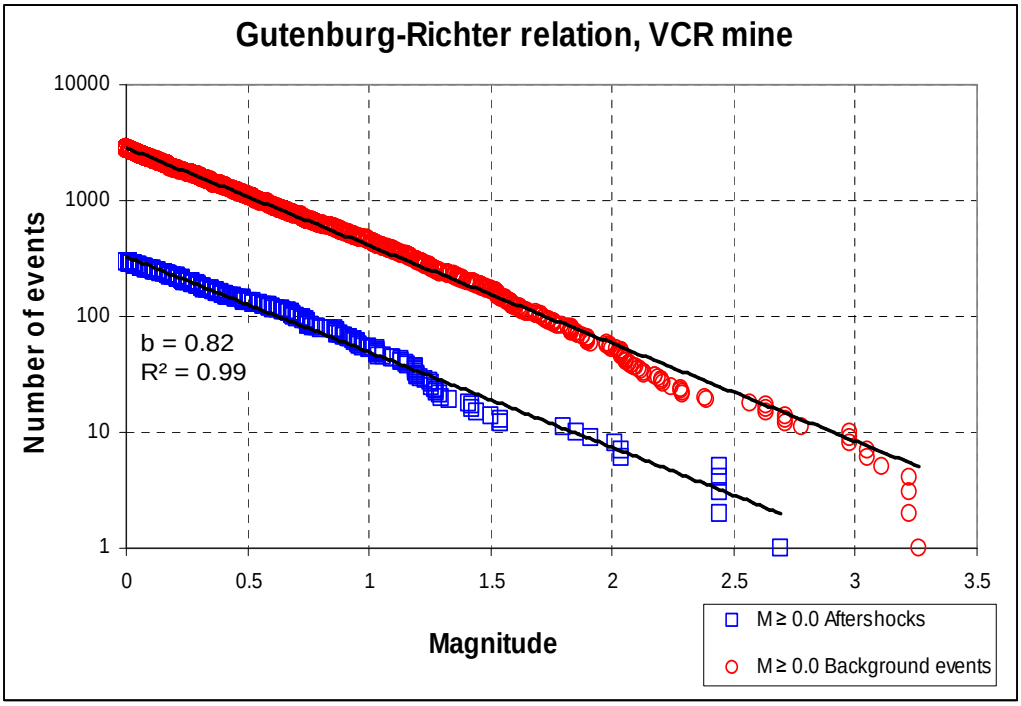

Figure 4.1:Gutenburg-Richter frequency-magnitude relation of aftershock and background seismicity at the VCR mine.

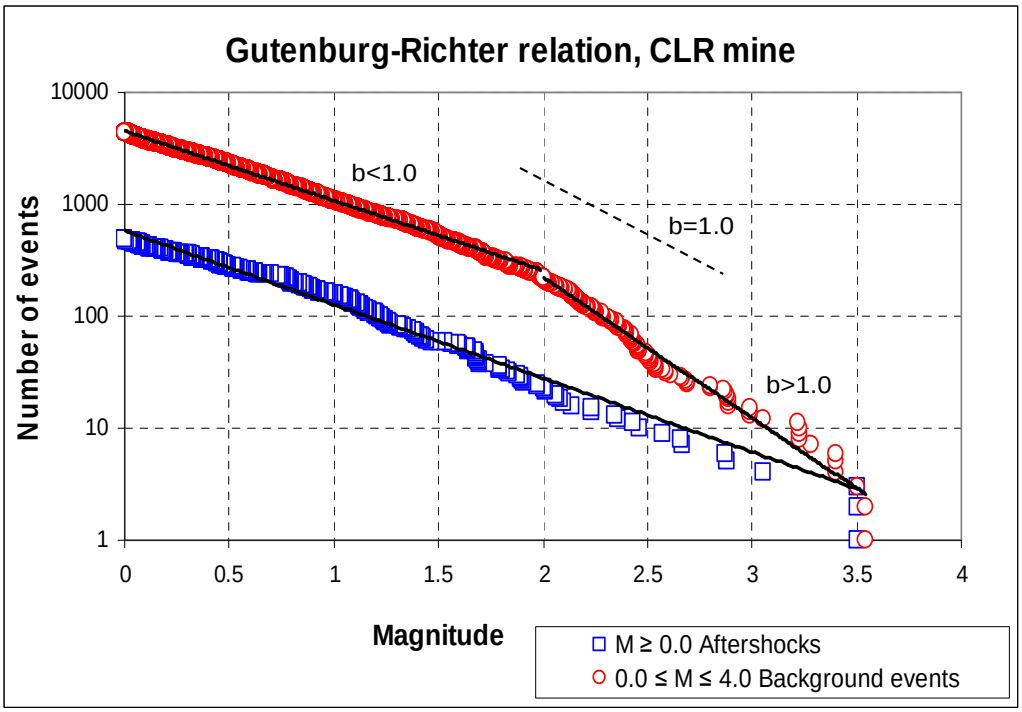

Figure 4.2: Gutenburg-Richter frequency-magnitude relation of aftershock and background seismicity at the CLR mine.

The data shows an upper magnitude limit for the aftershock data (around M = 3.0) and background data (around M = 3.5). Table 4.1 and Table 4.2 give the summary of the data parameters and the estimates of the *a*- and *b* values of the Gutenburg-Richter frequency-magnitude determined by the methods of least squares and maximum likelihood.

Table 4.1: Least squares estimates of the *a*- and *b*-parameters of the Gutenburg-Richter frequency-magnitude relation for the VCR and CLR mines.

Ventersdorp contact reef		
Parameter	Aftershocks	Background
N	297	2819
$M_{\min}$	0	0
b	0.82	0.84
a	2.47	3.45
Carbon Leader reef		
N	480	4362
$M_{\min}$	0	0
b	0.65	0.62 ($M_L \leq 2.0$) 1.25 ($M_L \geq 2.0$)
a	2.76	3.65 ($M_L \leq 2.0$)

Table 4.2: Maximum likelihood estimate of the *b*-parameter of the Gutenburg-Richter frequency-magnitude relation (VCR).

Ventersdorp Contact reef		
Parameter	Aftershocks	Background
N	297	2819
$< M >$	0.57	0.52
$M_{\min}$	0	0
$\hat{\beta}$	1.74	1.92
95 % confidence	$1.55 \leq \hat{\beta} \leq 1.95$	$1.85 \leq \hat{\beta} \leq 1.99$
b	0.76	0.83
σ	0.04	0.02

Table 4.3: Maximum likelihood estimate of the *b*-parameter of the Gutenburg-Richter frequency-magnitude relation (CLR).

Carbon Leader reef		
Parameter	Aftershocks	Background
N	480	2819
$< M >$	0.57	0.52
$M_{\min}$	0	0
$\hat{\beta}$	1.2	1.4
95 % confidence	$1.17 \leq \hat{\beta} \leq 1.39$	$1.39 \leq \hat{\beta} \leq 1.47$ ($M_L \leq 2.0$)
b	0.56	0.71 ($M_L \leq 2.0$) 1.27 ($M_L \geq 2.0$)
σ	0.03	0.01

The least squares estimate of the aftershock and background data show no large difference in the *b*-values with $b_A \approx 0.82$ and $b_B \approx 0.84$ for aftershock and background seismicity respectively for the VCR data. A similar behaviour is observed for the CLR data with $b_A \approx 0.65$ and $b_B \approx 0.62$ for aftershocks and $M \leq 2.0$ background seismicity respectively. Background data from the CLR mine however shows a different behaviour in that it exhibiting a bi-modal distribution evident from the change in the b-value at about $M_L = 2.0$ from $b = 0.62$ to $b = 1.25$. Further analysis was done to check if the bi-modal distribution about $M_L = 2.0$ was an artefact of the minimum mainshock magnitude ($M_{main} \geq 2.0$) chosen for the analysis. The same behaviour was still observed for different minimum mainshock magnitudes. The Gutenburg-Richter frequency-magnitude relation satisfactorily fits the aftershock and background data from the two mines.

A more detailed comparison using the maximum likelihood method shows that the *b*-values (for the aftershocks and background data) are statistically different from each other at 95% confidence when considering their standard deviations.

4.3. Conclusions

Mine tremor aftershocks, similarly to natural earthquake aftershocks, obey the Gutenburg-Richter frequency-magnitude relation with b-values close to 1.

Although the b-values of the aftershock and background data are approximately equal, statistical comparison of the aftershock and background data shows a statistically significant difference when compared at the 95% confidence level. In practical terms this difference is not large enough to indicate different physical processes. The approximately equal b-values suggest that the mechanisms involved in the generation process for the two groups are the same.

The phenomenon of bi-modal distribution evident in the background data from the CLR mine has been previously observed in mine events. It can be attributed to factors such as different source mechanisms, site effects or breakdown in self-similarity (Sellers et al., 2005). Understanding of this phenomenon of mine events still requires further research.

CHAPTER 5. BÅTH'S LAW

5.1. Introduction

The relationship between a mainshock and its largest aftershock was studied by Båth (1965). Båth (1965) found that the magnitude difference between a mainshock and its largest aftershock was, on average, 1.2 magnitude units (equation 2.5). The importance of Båth's law is clear as it attempts to anticipate the magnitude of the largest aftershock following a mainshock, that is, is the aftershock likely to be damaging.

Although some studies have validated the application of Båth's law to natural earthquakes, discrepancies have also been found on other studies. The model by Console et. al. (2003), where all events are assumed to belong to the self-similar set of earthquakes following the Gutenburg-Richter distribution, shows a large dependency of ΔM on the magnitude thresholds chosen for mainshocks and aftershocks. Here we test the validity of Båth's law for mine aftershocks.

5.2 Results and discussions

The investigation of the applicability of Bath's law to mine aftershocks was performed on aftershocks within 400m of and 1 hour following M ≥ 2.0 mainshocks. The extended time window and distance at the VCR mine was done to accommodate the small number of events. The selection criterion ensures that aftershocks are not contaminated by the background seismicity. The figure below shows data from the VCR mine where mainshocks are plotted along with their largest aftershock succeeding them. On average the value of ΔM is found to 1.57 ± 0.59. Also shown on the figure are the line representing Bath's ΔM = 1.2 and ΔM = 1.57 found for mine aftershocks. Similar results are obtained for the CLR mine with ΔM = 1.66 ± 0.68 (Figure 5.2).

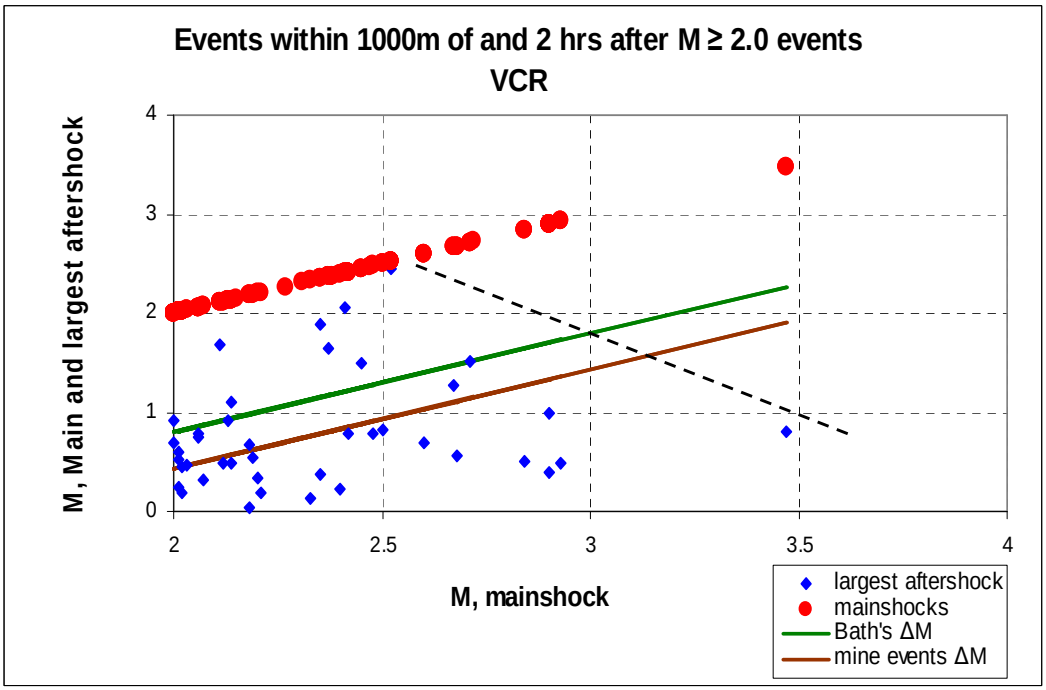

Figure 5.1: Bath's law analysis of M ≥ 0.0 aftershocks within 1000 m of and 2 hour following 163 M ≥ 2.0 mainshocks (VCR mine).

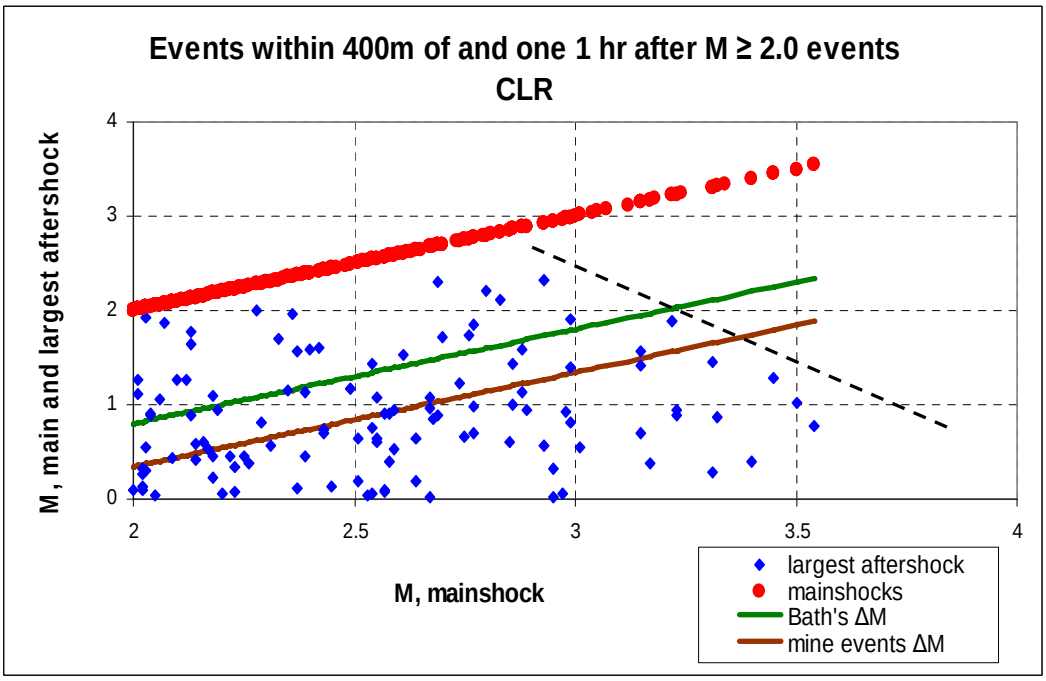

Figure 5.2: Bath's law analysis of M ≥ 0.0 aftershocks within 400 m of and 1 hour following 517 M ≥ 2.0 mainshocks (CLR mine).

A noticeable trend from the two figures is the gradual increase of ΔM with increasing mainshock magnitude around M ≥ 3, which is more pronounced at the CLR (Figure 5.3). Because of the use of lead and lags and regional stabilizing pillars to limit the extent of ruptures (Durrheim et. al., 1998) and reduce the sizes of ESS lobes (Jager and Ryder, 1999, pg 53), larger seismic events tend to occupy the entire source area resulting in little residual ESS (ESS measures the levels of shear stresses on planes of weaknesses) being released as aftershocks.

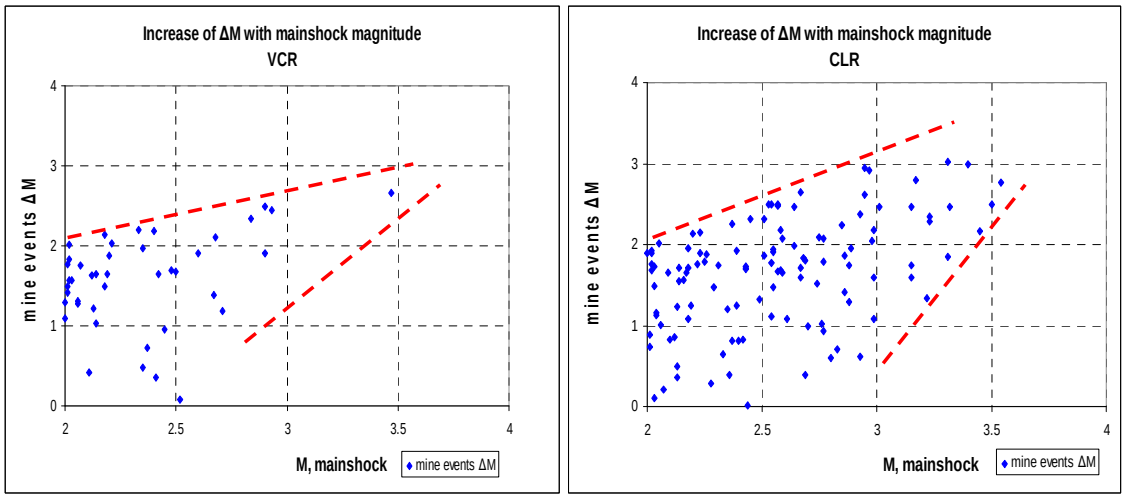

Figure 5.3: Increase of ΔM with increasing mainshock magnitude.

5.3 Conclusions

It was found that Bath's law was not applicable to mine aftershock. The average magnitude difference between a mainshock and its largest aftershock found to be greater than that predicted by Bath's law. Furthermore it was found that the magnitude difference tends to increase as the mainshock magnitude increases, notably at about 3.0.

The increase in ΔM, suggests that the larger events (with M ≥ 3.0) tend to be succeeded by smaller magnitude aftershocks. This behaviour is due to the exhaustion of the ESS lobes as larger events tend to occupy the entire source area, which is limited by the panel length. This results in little residual ESS being released as aftershocks since the panel length reduces the sizes of ESS lobes.

CHAPTER 6. MODIFIED OMORI LAW

6.1. Introduction

To propose a methodology of assessing the seismic hazard associated with aftershocks, the Modified Omori law was used to estimate time periods following larger seismic events during which re-entry to working areas should be postponed.

The decay of aftershock occurrence with time was studied by Omori (1894) and found that it was inversely proportional to the time following the mainshock (i.e. rate ~ 1/t). This simple relation was later modified by Utsu (1961) with an addition of the constants *c* and *p* (equation 6.1).

$$n(t) = \frac{K}{(t+c)^p} \tag{6.1}$$

t is the time after the mainshock, *n(t)* is the number of events occurring at time *t*, *K* and *c* are parameters and p is a rate constant of aftershock decay (Nanjo et al., 1998) and has a value close to 1.

Although the Modified Omori model is widely accepted by seismologists, other functions have also been found to fit the aftershocks decay rates (e.g. Gross and Kisslinger, 1994).

Although the equation proposed by Omori (1894) in its simplest form is a reasonable approximation of the aftershock decay, it results in a singularity at the time of a mainshock (i.e. t=0). The addition of a constant *c* to the original form avoids the singularity but has also been questioned whether it bears any physical meaning or if it is simply due to instrumental inadequacy (Kagan, 2004). Kagan (2004) suggested that the c-parameter is due to missing aftershocks, especially those with small magnitudes as their detection is obstructed by the mainshock coda waves directly after its occurrence. Analysis by Shcherbakov et. al. (2006) showed that *c* increases with decreasing lower aftershock magnitude cut-off and suggested that it characterizes the time for the establishment of Gutenburg-Richter scaling for aftershocks.

6.2. Results and discussions

6.2.1 Effect of bin size on aftershock event rate

The aftershock stacking procedure described in chapter 3, explained how aftershocks are binned into time and distance bins. This discussion investigates how the binning procedure, specifically the number of events in each bin affects the calculation of the event rate.

The limits of each time bin were adjusted to ensure that each bin contained the same number of events. The end of the bin was moved until the specified number of events was found. The time for each bin is given by the average time of events in each bin. The event rate, expressed as the number of aftershocks per day, is calculated by dividing the number of events in each bin by the difference between the start and end times of the bin. The event rate is normalised by the number of mainshocks used in the particular analysis. Figure 6.1 is a plot of aftershock decay rate with time following the mainshock. Plotted on the same graph are the event rates computed using bins with size 5, 10, 20 events per bin. As expected the larger number of events per bin results in a smooth decay curve. Beyond 100 000 seconds, the bin size was increased as the time or distance from the mainshock increased to adjust for large number of events at late times (since the log-log scale is used).

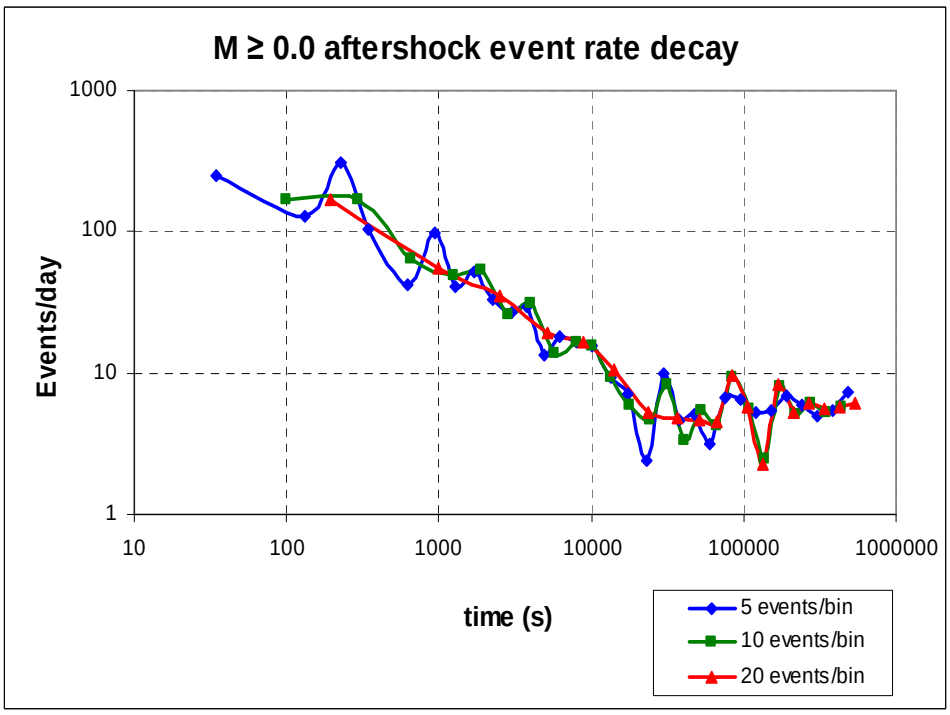

Figure 6.1: Effect of number of events per bin on the event rate decay curve.

The number of events per bin has a trade-off effect between statistical accuracy and temporal resolution with the general decay trend still preserved. Small number of events per bin increases the number of points on the curve giving a better temporal resolution, while increasing the number of events per bin reduces the number of points on the curve but giving better statistical accuracy.

6.2.2 Influence of blasting on aftershock event rate

As discussed in chapter 3.2, seismicity doubles following the onset of blasting. This increased rate of seismicity also manifests in the aftershock decay rate and is clearly identifiable at later times (shaded area in figure 6.2). To estimate the background rate, the influence of blasting is corrected by averaging over the long-term seismicity rate (seismicity occurring at later times after the aftershock decay) and then halving the rate (Figure 6.2). The result is the background rate which would have been followed if there had been no influence of blasting events.

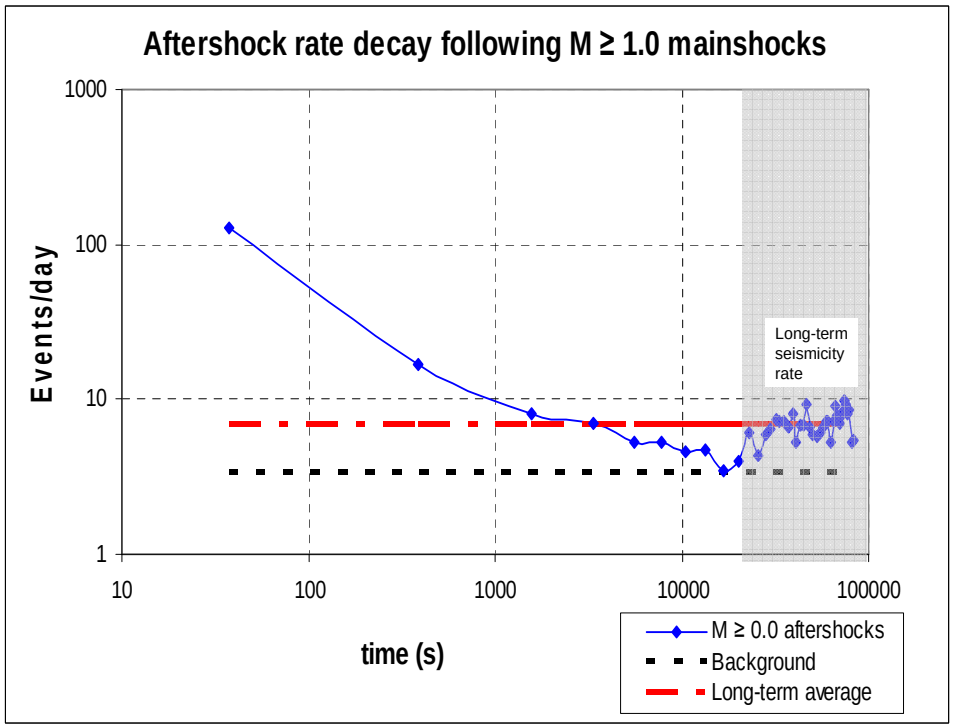

Figure 6.2: Estimation of the background rate. Long-term average determined by averaging over long-term seismicity (shaded area).

6.2.3 Omori c-parameter

To determine the c-parameter, aftershock magnitudes are plotted against their occurrence time following the mainshock (Figure 6.3 and Figure 6.4). The c-parameter, demonstrated by the time delay following the mainshock, shows that small magnitude aftershocks are not detected immediately following the mainshock. This suggests that the c-parameter has no physical significance but is an instrumentation artefact caused by the system-triggering logic. This is due to the automatic adjustments in the triggering algorithm of the system.

Figure 6.3 shows the determination of the c-parameter from the plot of aftershock magnitude against their occurrence time following the mainshock. The data shows that the recording systems take at most 20 seconds to achieve catalogue completeness following a larger event for aftershock cut-off magnitude of M_c= 0.0. Figure 6.3 (b) demonstrates that this time increases with decreasing aftershock minimum threshold magnitude. Figure 6.4 shows a similar behaviour for aftershocks at the VCR mine.

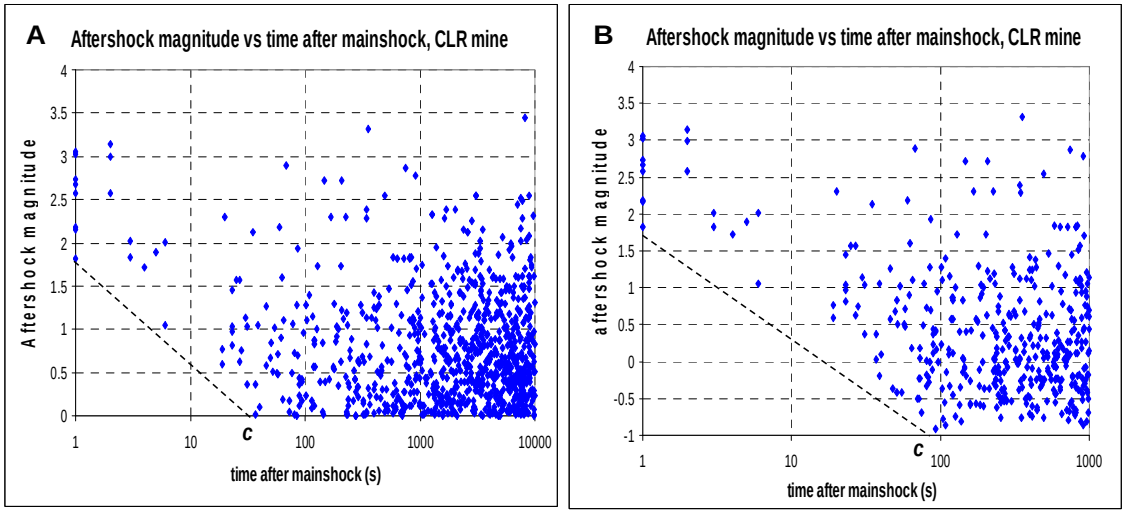

Figure 6.3: Time-magnitude distribution of aftershocks (CLR mine).

(A) Aftershocks with cut-off magnitude Mc = 0.0. (B) Aftershocks with cut-off magnitude Mc = -1.0.

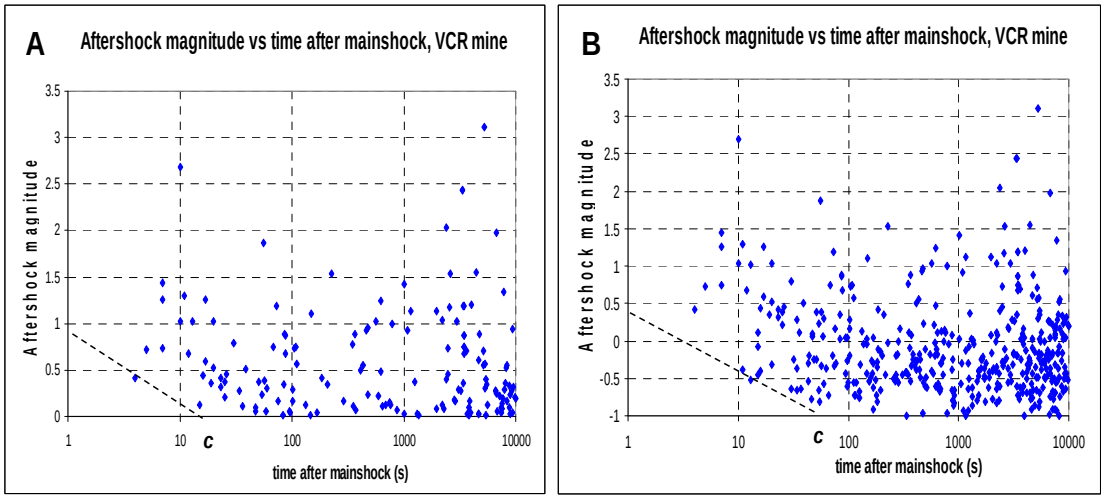

Figure 6.4: Time-magnitude distribution of aftershocks (VCR mine).

(A) Aftershocks with cut-off magnitude M_c = 0.0. (B) Aftershocks with cut-off magnitude M_c = -1.0.

The interpretation of the c-parameter as an instrumentation artefact is in agreement with Kagan (2004). Furthermore its increase with aftershock magnitude cut-off also agrees with Shcherbakov et. al. (2006).

6.2.4 Aftershock event rate

The decay rate of aftershocks following mainshocks with magnitude threshold M = 1.0, M = 2.0 and M = 3.0 are shown in figure 6.5. Aftershocks with minimum magnitude M = 0.0 within 1 day and 1000 m of the mainshock were considered. The p-values are estimated by fitting a least squares regression line through the event rate curve. Figure 6.6 investigates the rate decay of

different lower aftershock threshold magnitudes. The zone of influence of the mainshock on the rate decay shows no significant influence of the p-values (Figure 6.5).

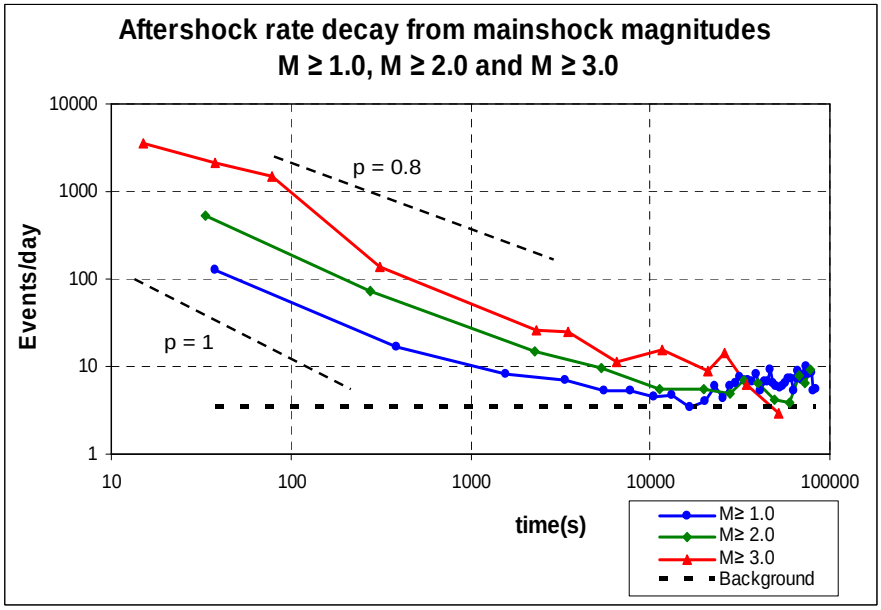

Figure 6.5: M ≥ 0.0 aftershock rate decay following mainshocks with threshold magnitudes M ≥ 1.0, M ≥ 2.0, and M ≥ 3.0. The lines representing p = 1 and the estimated background level are also shown.

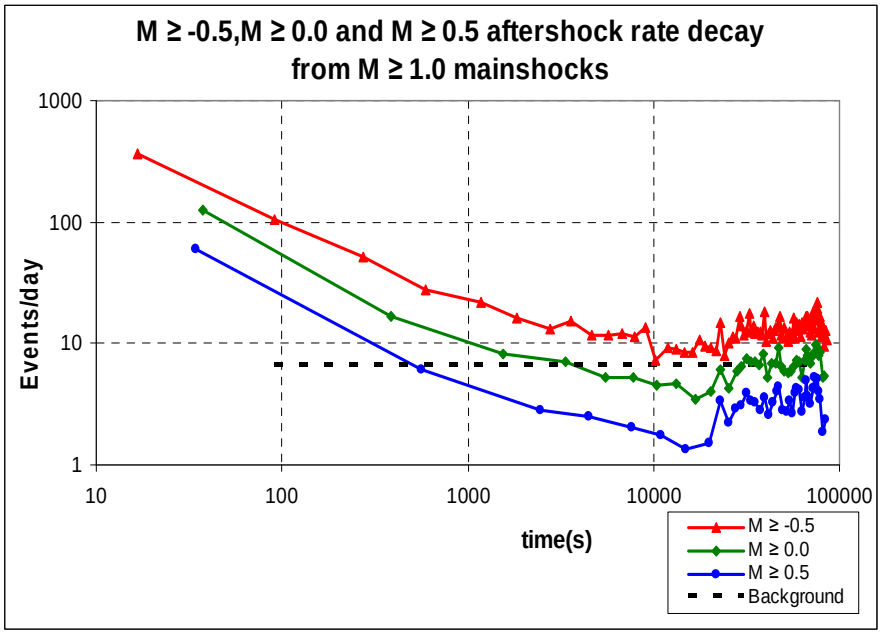

Figure 6.6: M ≥ -0.5, M ≥ 0.0 and M ≥ 0.5 aftershock rate decay following mainshocks with magnitude M ≥ 1.0. The line representing the estimated background level is also shown.

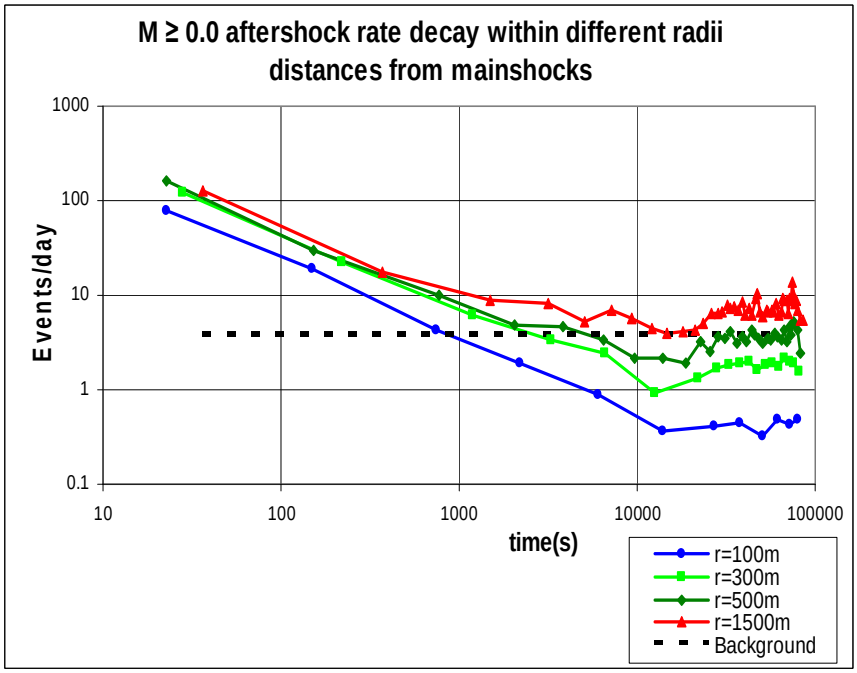

Figure 6.7: M ≥ 0.0 aftershock rate decay within different radial distances from M ≥ 1.0 mainshocks. The line representing the estimated background level is also shown.

The above results have been giving rates calculated within a fixed distance from the mainshock (1000 m). The results can be extended to two-dimensions by calculating the event rate within distance bins from the mainshock. This allows for simple and quick estimations of the rate within certain times and distances following the mainshock.

Figure 6.8 and Figure 6.9 give contour plots of the events rate versus time and distance following 2.0 ≤ M ≤ 3.0 and 3.0 ≤ M ≤ 4.0 mainshocks at the VCR mine. The contours represent the rate presented on a logarithmic scale

with a minimum rate of 0.1 events/day. A similar behaviour is also observed for aftershocks at the CLR mine (Figure 6.10 and Figure 6.11).

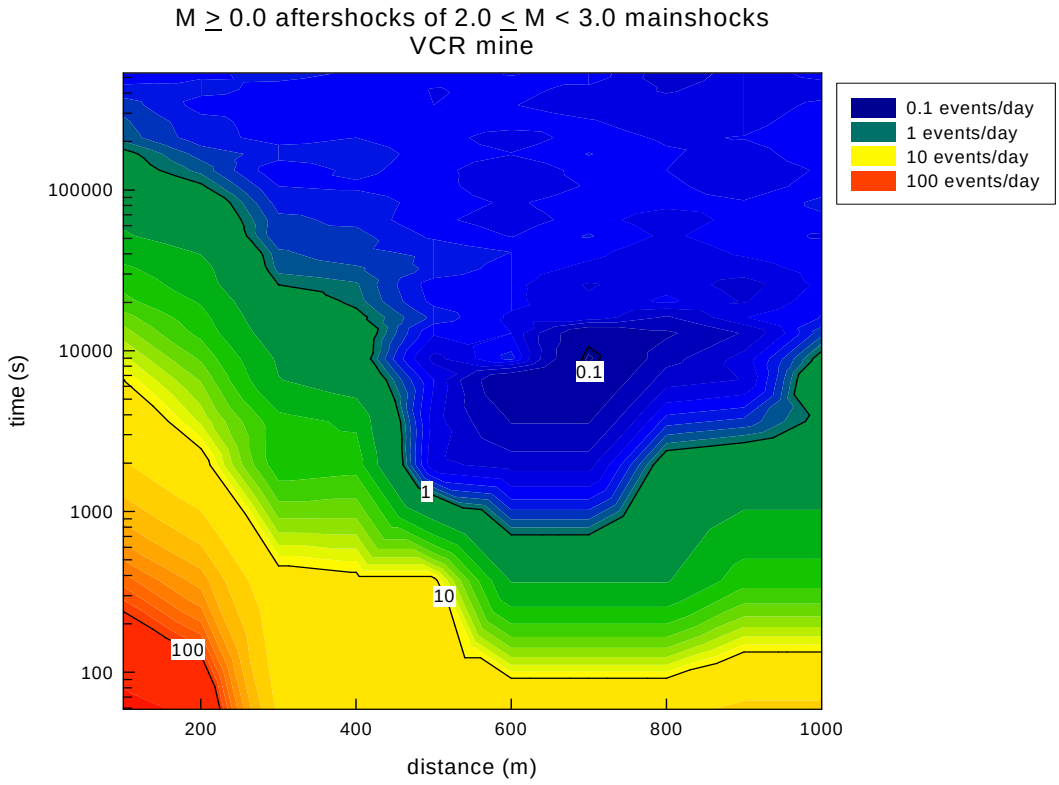

Figure 6.8: Event rate contour plots as a function of time and distance from 2.0 ≤ M ≤ 3.0 mainshocks (VCR mine).

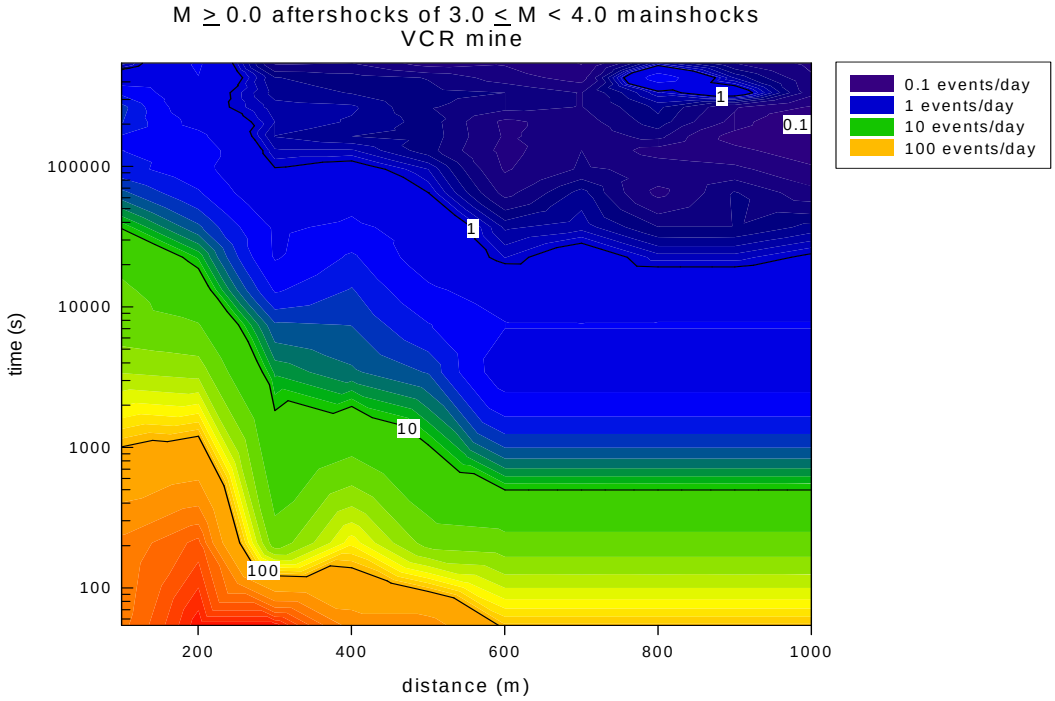

Figure 6.9: Event rate contour plots as a function of time and distance from 3.0 ≤ M ≤ 4.0 mainshocks (VCR mine).

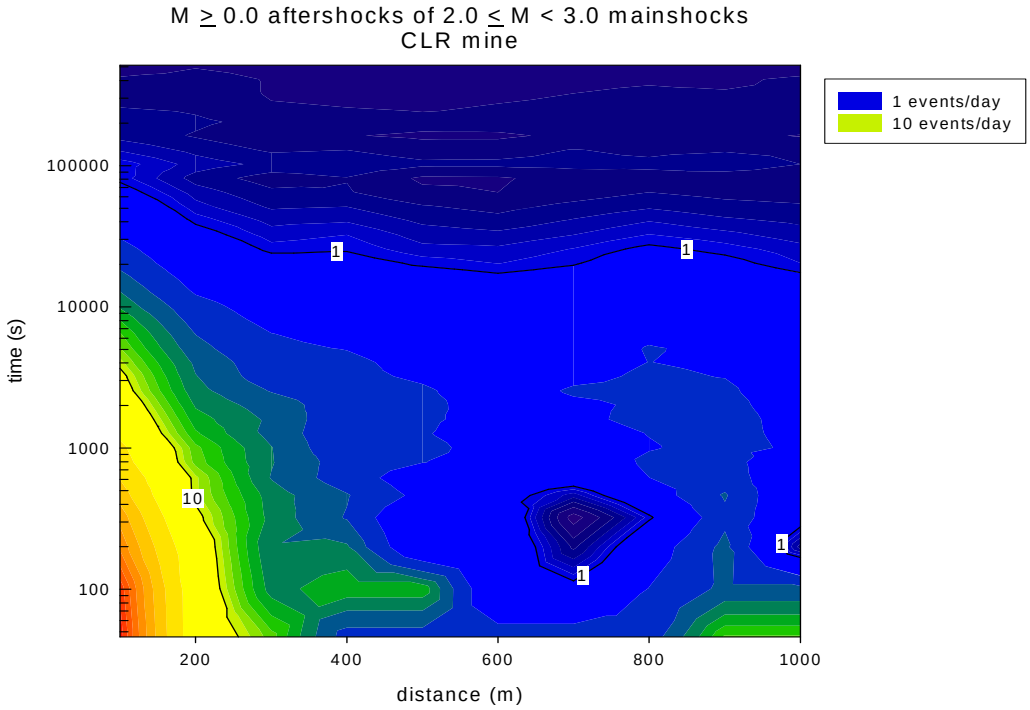

Figure 6.10: Event rate contour plots as a function of time and distance from 2.0 ≤ M ≤ 3.0 mainshocks (CLR mine).

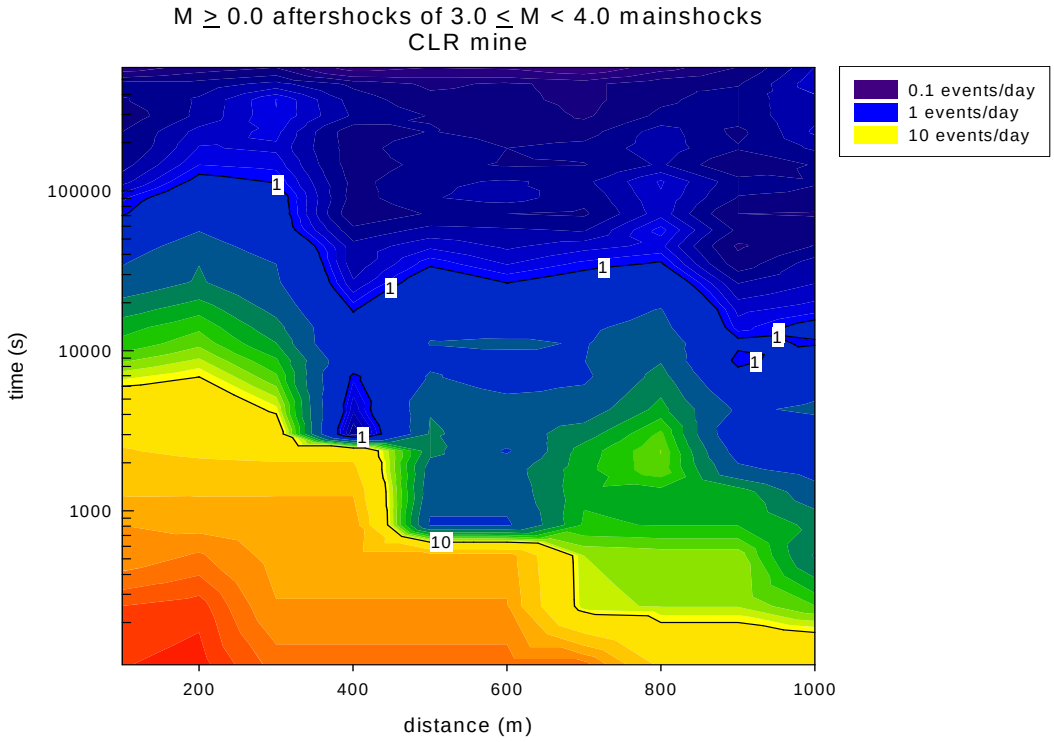

Figure 6.11: Event rate contour plots as a function of time and distance from 3.0 ≤ M ≤ 4.0 mainshocks (CLR mine).

Proposing a methodology of assessing the hazard posed by aftershocks following the mainshock, the events rate curves are used to identify time periods for which the rate has decreased to acceptable levels (Figure 6.12). The dashed lines *A* and *B* are used to determine time periods where the rate is 10× and 3× the estimated background rate respectively.

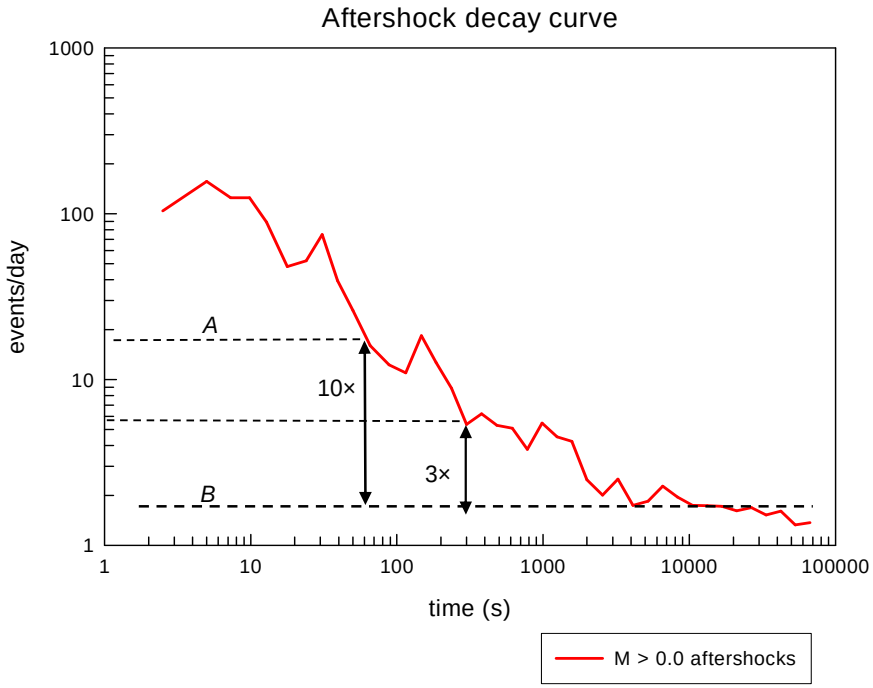

Figure 6.12: Determination of time periods where the event rate has decreased to background levels.

Using this method, a table giving the time periods when the rate is 10× and 3× the background as a function of time and distance ranges from the mainshock was constructed (Table 6.1). The rate of 10× and 3× background were chosen to demonstrate the principle of the method. In practice the rates used as benchmarks should be selected through a consultative process involving employees, labour and regulators.

Due to small sample statistics encountered for larger events, re-entry times tend to be larger. Time periods marked with an asterisk are less reliable as

they are due to small number of aftershocks. In practice, time periods greater than 1 hour will possibly lead to a loss of a working shift.

Table 6.1: Time periods required for the aftershock event rate to reach 10× and 3× the background rate.

VCR mine	**10 ×** **time in minutes**		**3 ×** **time in minutes**	
D (m) M_{main}	0-200	200-400	0-200	200-400
1.0 ≤ M < 2.0	5	2	24	30
2.0 ≤ M < 3.0	16	5	180	162
3.0 ≤ M < 4.0	48	60	300	480 *
CLR mine	**10 ×**		**3 ×**	
D (m) M_{main}	0-200	200-400	0-200	200-400
1.0 ≤ M < 2.0	3	2	16	78 *
2.0 ≤ M < 3.0	10	3	48	15
3.0 ≤ M < 4.0	60	24	120	120*

Note: asterisk indicates less reliable time periods as they are due to small number of aftershocks.

Aftershock event rate increases with increasing mainshock magnitude and increases as the minimum threshold magnitude for aftershocks decreases.

The radius of influence does not significantly affect the event rate. The data also shows that varying these parameters has no influence of the decay rate exponent p, which has values close to 1. The contour plots show that the event rate increases with increasing mainshock magnitude. As an example for $2.0 \leq M < 3.0$ mainshocks (figure 6.8), a 100 events/day contour is reached after about 3 minutes and around 200 meters of the mainshock. For $3.0 \leq M < 4.0$ mainshocks the contour is reached after about 16 minutes and around 600 meters from the mainshock.

The results given in Table 6.1 also agree with the above results that the time taken for the rate to reach a specific level (e.g. 10× or 3× the background) decreases as the distance ranges from the mainshock increases. Because of a small number of larger magnitude aftershocks, time periods for $3.0 \leq M \leq 4.0$ mainshocks tend to be longer.

6.3. Conclusions

The c-parameter for mine aftershocks shows an increase with a decreasing aftershock cut-off magnitude, consistently at the two mines. Furthermore it is found that *c* has no physical significance but results from instrumentation inadequacy. This is in agreement with the suggestion by Kagan (2004).

The rate decay of mine tremors aftershocks was found to follow the Modified Omori law with p-values close to unity. Mainshocks are followed by an increased rate of seismicity immediately after their occurrence, typically in excess of 1000 events/day for M ≥ 3.0 mainshocks. Using Omori's law, tables giving time period taken for the rate to decrease to background levels can be constructed. These tables can be used as guidelines for re-entry times into working areas after the occurrence of a seismic event.

CHAPTER 7. AFTERSHOCK DENSITY DECAY

7.1 Introduction

The physics of aftershock triggering has been mostly understood in terms of static stress transfer and used to explain the distribution of aftershocks around a mainshock (Ganas et. al, 2008). Earthquake triggering is generally classified into three stress transfer modes; Static stress, Quasi-static stress and Dynamic stress transfer modes (Hill, 2007). Static and quasi-static triggering is explained by the Coulomb failure criterion. Triggering is caused by the stress changes loaded by the mainshock in the vicinity of a fault which is close to its Coulomb failure threshold.

Static stresses decay rapidly with distance as r^{-3} and hence their triggering potential is limited to one or two source dimensions (Hill, 2007). Quasi-static stress, which is due to viscous relaxation of the crust following an earthquake, decay more slowly with distance as r^{-2}. Their triggering potential extends to greater distances and because of their low viscoelastic propagation speeds, they can result in delayed triggering (Pollitz and Sacks, 2002). Although these models succeeded in explaining aftershock triggering in the near field, triggering has also been evident at distances much greater than the triggering potential of the two models.

The dynamic stress model offers an explanation for this phenomenon. Dynamic stresses propagating as seismic waves have the potential to trigger seismicity from the near field to greater distances than the other two modes. The amplitudes of dynamic stresses decrease slowly with distance as r^{-2} for body waves and $r^{-1.5}$ for surface waves (Hill, 2007). Because dynamic stresses are oscillatory, bringing stresses further from or closer to the Coulomb failure of a fault, they result in no permanent stress changes. A study by Felzer and Brodsky (2006) on aftershock density supported dynamic triggering as the density was found to fall-off with distance as $r^{-1.3}$, comparable to the decay of maximum seismic wave amplitude, a proxy for dynamic stress.

To understand the triggering mechanism of mine tremor aftershocks, aftershock density decay was measured with distance from the mainshock. The density is measured by determining the frequency of aftershocks within given distances. The density data points are plotted at the centre of each bin.

7.2 Results and discussions

A time window of one week was selected for the analysis. The longer time period allows for better background correction. Events within two hours of the mainshock were selected as possible aftershocks and the other events taken as the background. Aftershock density (expressed as events/min) was normalised to background density. Aftershock density fall-off with distance

was determined from the ratio of the normalised number of aftershocks to the density decay predicted by two numerical models of the mining-induced seismicity (Spottiswoode et al., 2008). Numerical models are essential as they solve problems which cannot be solved analytically, allow for analysis of the rockmass under different conditions, and allow for confirmation of assumed rockmass behaviour.

The “active” model considers the strain energy released by recent mining to be the principal driver of both mainshocks and aftershocks. An area is defined as “active” if mining took place in the month prior to the mainshock. The normalised number of events predicted by this model was found to be similar to the observed background seismicity (green circles in figure below). Similar results are obtained for the VCR data. The density fall-off with distance is well fitted by a power law:

$$\rho(r) = Ar^{-q} \tag{7.3}$$

where A is a constant which depends on the number of aftershocks. The decay exponent is q = 1.37 for the CLR data and q = 1.34 for the VCR data. The line representing the fall-off that would have been followed if the triggering was due to static stresses is also shown on the figures.

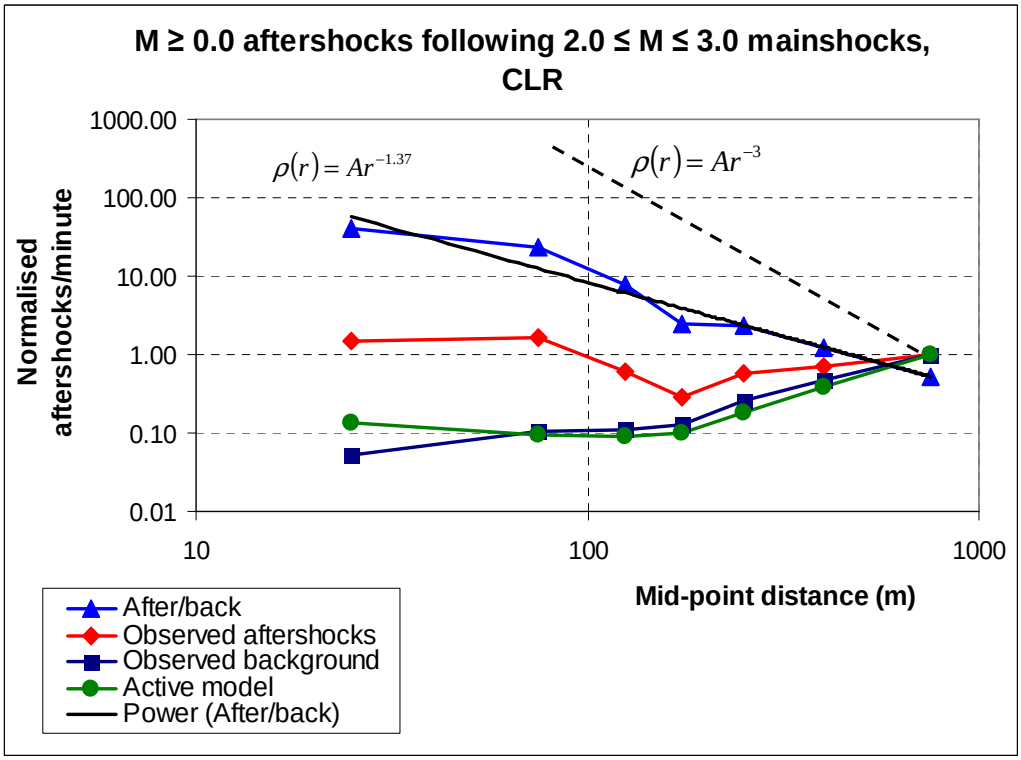

Figure 7.1: Aftershock density as a function of distance from the mainshock.

The background seismicity is modelled as a function of strain energy released associated with “active mining”.

The “stationary” model (applied to the same data as figure 7.1) considers the possibility that aftershocks may also be triggered in the stressed ground around old mining faces. On-reef stress in excess of 300 MPa was considered to be sufficiently stressed to be in a state of incipient failure. The normalised number of events in this model is considerably smaller than the observed background seismicity (green circles and blue squares in figure 7.2). A fit to the data shows a constant fall-off as $r^{-1.62}$.

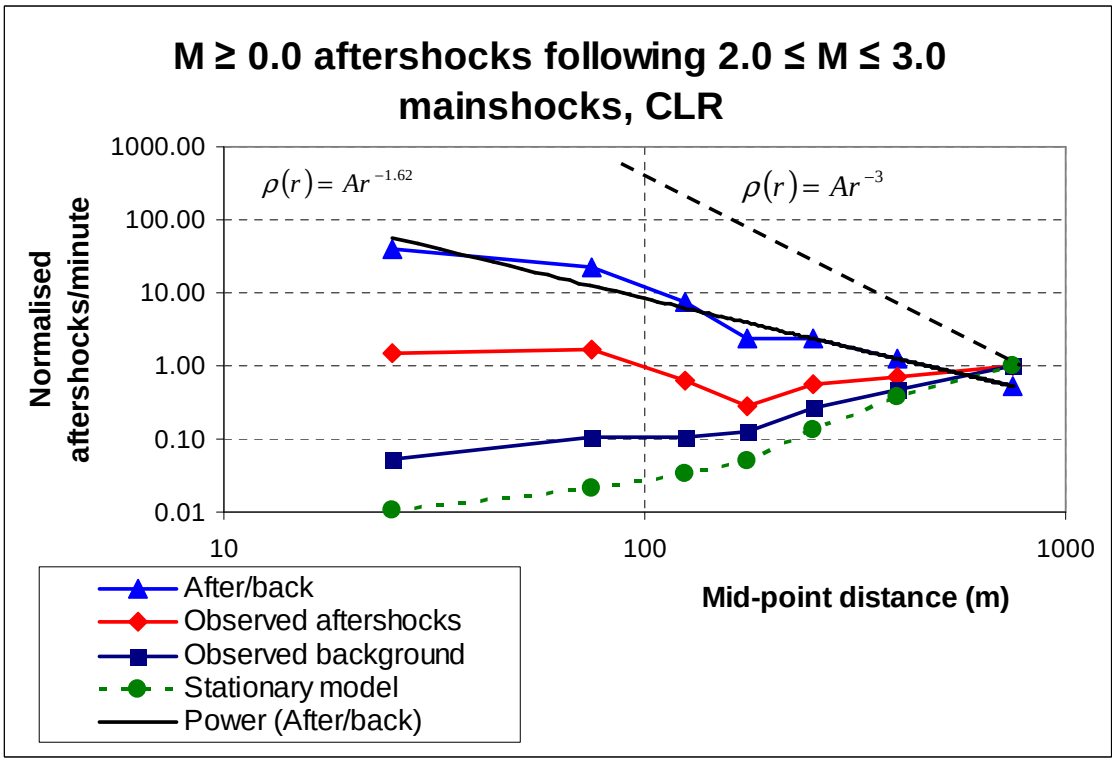

Figure 7.2: Aftershock density as a function of distance from the mainshock.

The background seismicity is modelled as a function of strain energy released associated with “stationary mining”.

Density decay with distance shows a much slower $r^{-1.37}$ fall-off when considering active mining as the driver of aftershocks. The fall-off increases to $r^{-1.6}$ when considering aftershocks to be triggered in the stressed ground in the vicinity of old mining faces. Both models support the dynamic triggering mode as the driver for aftershock triggering. The decay exponents are similar to those determined by Felzer and Brodsky (2006) in the study of natural earthquake aftershocks.

7.3. Conclusions

Aftershock density is found to fall-off with distance as $r^{-1.3}$ in both the CLR and VCR datasets. This fall-off rate is similar to that of Felzer and Brodsky (2006) for natural earthquake aftershocks. The analysis, like that of Felzer and Brodsky (2006), supports the notion that most aftershocks are triggered by dynamic stresses rather than by quasi-static stress redistribution. The results supports the conclusion of Spottiswoode et al. (2008) that seismicity is driven primarily by the strain energy changes due to active mining, rather than by high stresses, which are found in both active and old mining environments.

CHAPTER 8. AFTERSHOCK PROBABILITY

8.1 Introduction

The probability of aftershock occurrence was studied by Reasenberg and Jones (1989) for hazard assessment following a mainshock. The method combines the Gutenberg-Richter relation and the Modified Omori law into a rate equation giving the rate λ of aftershocks with magnitude M or larger, at time *t* following the mainshock of magnitude M_m.

$$\lambda(t,M) = 10^{a+b(M_m - M)}(t+c)^{-p} \tag{8.1}$$

The various constants in the equation are as explained previously. Using equation 8.1, Reasenberg and Jones (1989) determined the probability of one or more aftershocks occurring in the magnitude range $M_1 \leq M \leq M_2$ and time range $t_1 \leq t \leq t_2$ (equation 8.2).

$$P = 1 - \exp[-\int_{M_1}^{M_2}\int_{t_1}^{t_2} \lambda(t.M)dtdM] \tag{8.2}$$

where the Omori equation integrates to;

$$O(t_1,t_2) = \begin{bmatrix} \dfrac{(t_2+c)^{1-p} - (t_1+c)^{1-p}}{1-p} \cdots (p \neq 1) \\ \ln(t_2+c) - \ln(t_2+c) \ldots (p=1) \end{bmatrix} \tag{8.3}$$

Equation 8.2 gives the aftershock probability as a function of parameters that describe an earthquake sequence, namely the initiating mainshock

magnitude, magnitudes of the succeeding aftershocks and their time of occurrence following the mainshock. In chapter 7, aftershock density fall-off was found to have an $r^{-1.3}$ dependency on the distance. The Reasenberg and Jones model (R & J model) is applied to mine aftershocks with modification to incorporate the density fall-off dependency on distance (equation 7.3).

The rate equation modified to incorporate the density decay law is then given by;

$$\lambda(t,r,M) = 10^{a+b(M_m-M)}(t+c)^{-p} r^{-q} \tag{8.4}$$

and the decay law integrates to

$$F(r_1, r_2) = \frac{r_2^{1-q} - r_1^{1-q}}{1-q} \ldots q \neq 1 \tag{8.5}$$

The exponent q = 1.34 and q = 1.32 for VCR and CLR respectively. The probability equation 8.2 then modifies to equation 8.6 below.

$$P = 1 - \exp[-\int_{M_1}^{M_2}\int_{t_1}^{t_2}\int_{r_1}^{r_2} \lambda(t,r,M)\,dt\,dr\,dM] \tag{8.6}$$

8.2 Results and discussions

The parameters used for the probability calculations are estimated for each sequence of the magnitude ranges considered. The Gutenberg-Richter parameters are estimated using the maximum likelihood method and the

p-values are determined from the Omori decay curves. Summaries of the parameters used are given in the tables below.

Table 8.1: Summary of the parameters used in the probability models (VCR mine).

VCR mine	**Input parameters**	
G-R relation	$2.0 \leq M_m \leq 2.5$	$3.0 \leq M_m \leq 3.5$
b	0.72	0.81
a	2.4	2.3
Modified Omori		
t	1 day	1 day
p	0.70	0.73
c	20	20
Density law		
q	1.34	1.34

Table 8.2: Summary of the parameters used in the probability model (CLR mine).

CLR mine	**Input parameters**	
G-R relation	$2.0 \leq M_m \leq 2.5$	$3.0 \leq M_m \leq 3.5$
b	0.59	0.57
a	2.7	1.8
Modified Omori		
t	1 day	1 day
p	0.55	0.68
c	20	20
Density law		
q	1.37	1.37

Figure 8.1 gives the aftershock probabilities determined from a stack of $2.0 \leq M \leq 2.5$ and $3.0 \leq M \leq 3.5$ mainshocks calculated using equation 8.6 for the VCR mine. Data from the CLR mine shows similar probability behaviour (Figure 8.2).

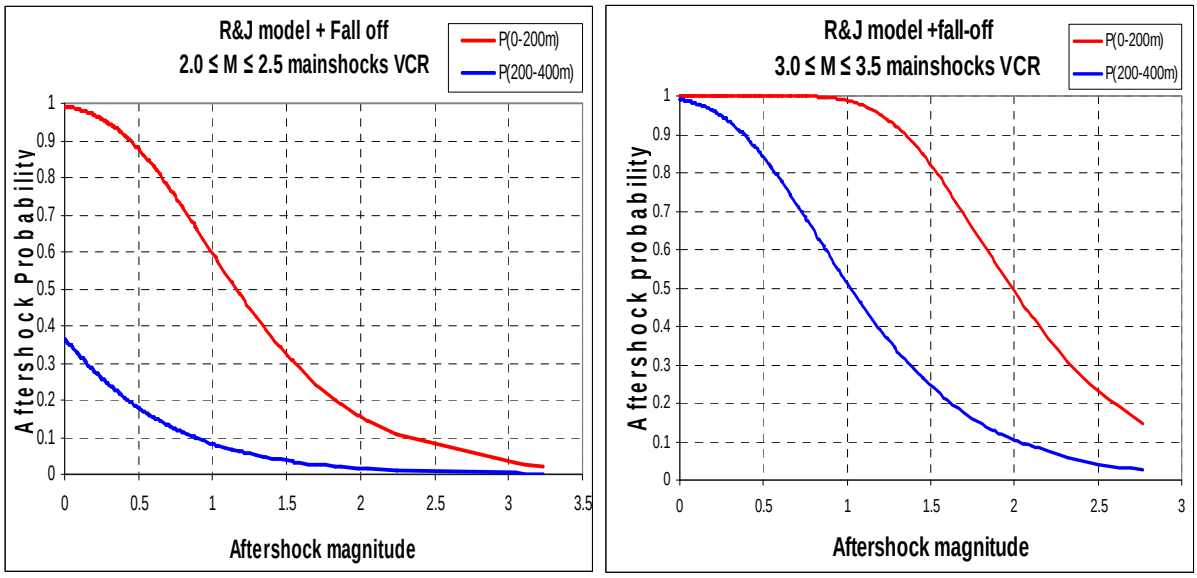

Figure 8.1: M ≥ 0.0 Aftershock probabilities for VCR mine within 1 day following, (a) 2.0 ≤ M ≤ 2.5 mainshocks and (b) 3.0 ≤ M ≤ 3.5 mainshocks) 2.0 ≤ M ≤ 2.5 mainshocks and (b) 3.0 ≤ M ≤ 3.5 mainshocks..

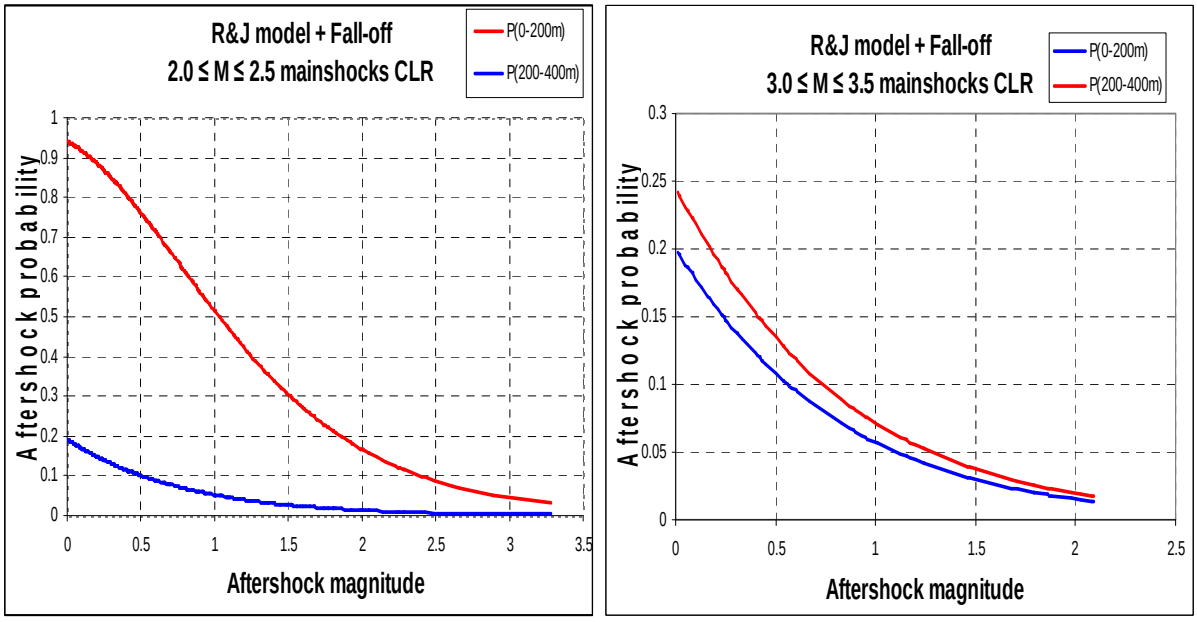

Figure 8.2: M ≥ 0.0 Aftershock probabilities for CLR mine within 1 day following, (a) 2.0 ≤ M ≤ 2.5 mainshocks and (b) 3.0 ≤ M ≤ 3 .5 mainshocks.

Aftershock probability is dependant on mainshock magnitude and distance and less so on time (i.e. probability is remains the same for time scales of minutes to hours). The probability increases as the mainshocks magnitude increases. Probabilities decrease drastically as the radii distance from the mainshock increases.

For $3.0 \leq M \leq 3.5$ mainshocks, the model shows a 50% probability of one or more $M \geq 2.0$ aftershocks occurring within 1 day and 0-200 m of the mainshock. For the same mainshock magnitudes, probability is four times less within 200-400 m of the mainshock. This indicates a high dependency of the probability on the distance. A similar behaviour is evident for the data from the CLR mine although the probabilities particularly for $3.0 \leq M \leq 3.5$ mainshocks show relatively low values compared to the CLR mine. This may be due to the small sample statistics as the small number of high magnitudes mainshocks are followed by a small number of aftershocks at that mine.

8.3. Conclusions

The Reasenberg and Jones model for aftershock probability has been modified to incorporate the density decay dependency of aftershocks on distance. The modified model gives the probability by considering all the parameters defining an aftershock sequence namely; the initiating mainshock magnitude, aftershock magnitude, time of aftershocks following the

mainshock and the distance decay of aftershocks. The model also incorporates all the relation defining aftershock sequences namely; the Gutenberg-Richter relation, Modified Omori law and the density law. The probability increases as the mainshocks magnitude increases and decrease with increasing distance from the mainshock. The high probability within 0 – 200 m of the mainshocks could be influenced by the fact that 200 m is within the source region for mainshock magnitudes considered with their approximate source length given by $\log_{10} L_s \approx \frac{M}{2} + 1$, where L_s is the source length in metres (Jager and Ryder, 1999, pg. 251).

CHAPTER 9. AFTERSHOCK PRODUCTIVITY

9.1. Introduction

Productivity of an earthquake relates to the amount of seismicity following the initiating mainshock. Persh and Houston (2004), in a study of deep crustal earthquakes, found that aftershock productivity showed a dependency on mainshock depth. In their study, productivity showed a decrease around 300 km and increased abruptly at around 550 km. These changes were correlated to a change in earthquake generation mechanism near 300 km depth and a major change in the rupture mechanism at around 550 km (Persh and Houston, 2004).

Yang and Ben-Zion (2009) found that for seismogenic zones with similar lithology, aftershock productivity showed an inverse relationship with mean heat flow (Figure 9.1).

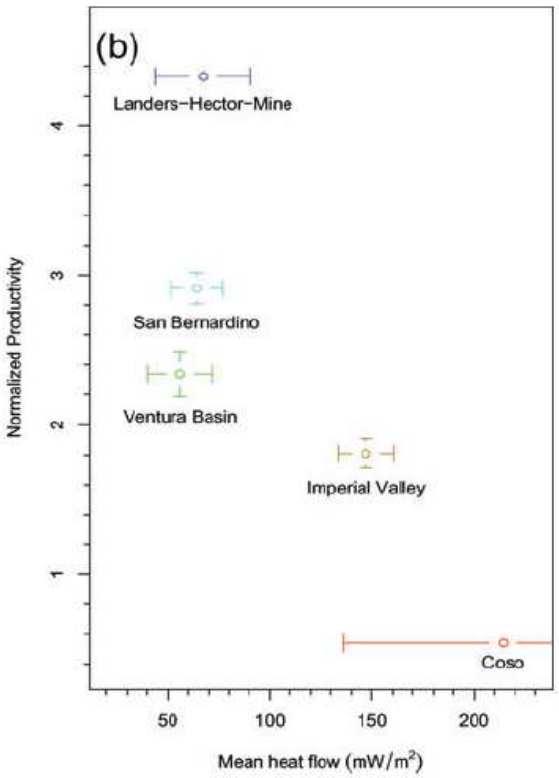

Figure 9.1: Dependency of aftershock productivity on mean heat flow for 5 regions in Southern California.

(From Yang and Ben-Zion (2009)).

Aftershock productivity is a useful parameter as it gives a measure of the anticipated seismicity following a mainshock. Mining provides a more controlled environment than natural tectonics and this enables us to study the influences of stresses, strains and geological features (faults and dykes) on aftershocks. It is known that seismicity has a dependency on these conditions (Ryder and Jager, 2002, pg. 254, Jager and Ryder, 1999, pg. 16). High ERR, high strain rates and geological features tend to increases seismicity. This chapter is focused on studying the dependency of aftershock productivity on

these mining conditions. This study is carried out to give insight into the science of the physical generation processes of aftershocks and the engineering implications of it.

To study the influences of these conditions, mainshocks were separated into three subsets defined by the mining conditions;

- Stress influences,
- Strain rate influences,
- Geological discontinuity influences.

In each subset mainshocks were divided into two groups based on their location with reference to the three conditions above. In each categorisation, mainshocks were divided into two contrasting groups (e.g. high stress environment versus low stress environment) based on their locations for each of the three conditions. These categorisations of mainshocks enable us to study the influence of the conditions on aftershock productivity. To study the stress influence, mainshocks locating in high stress environments are separated from those locating in low stress environments (Figure 9.2(A)). To study the strain influence, mainshocks locating at high strain environments (active faces) are separated from those locating in low strain environments (stationary faces) (Figure 9.2(B)). The influence of geological features is studied by separating mainshocks based on their proximity to geological features (Figure 9.2(C)).

The productivity of a mainshock is measured by the constant *K* of the Modified Omori law (equation 2.6). Productivity is then compared for the two mainshock populations of each subset to study its dependency on those mining conditions (Figure 9.2). In figure 9.2 (A), mainshock circled with a red colour is located in high a stress environment while those circled with a blue colour are located in a low stress environment. In figure 9.2 (B), mainshocks circled with a red colour are located in actively mined faces while that circled with a blue colour is located in a stationary face. In figure 9.2 (C), mainshocks circled with a red colour are located in close proximity of a dyke and a fault while those circled with a blue colour are located away from dykes and faults.

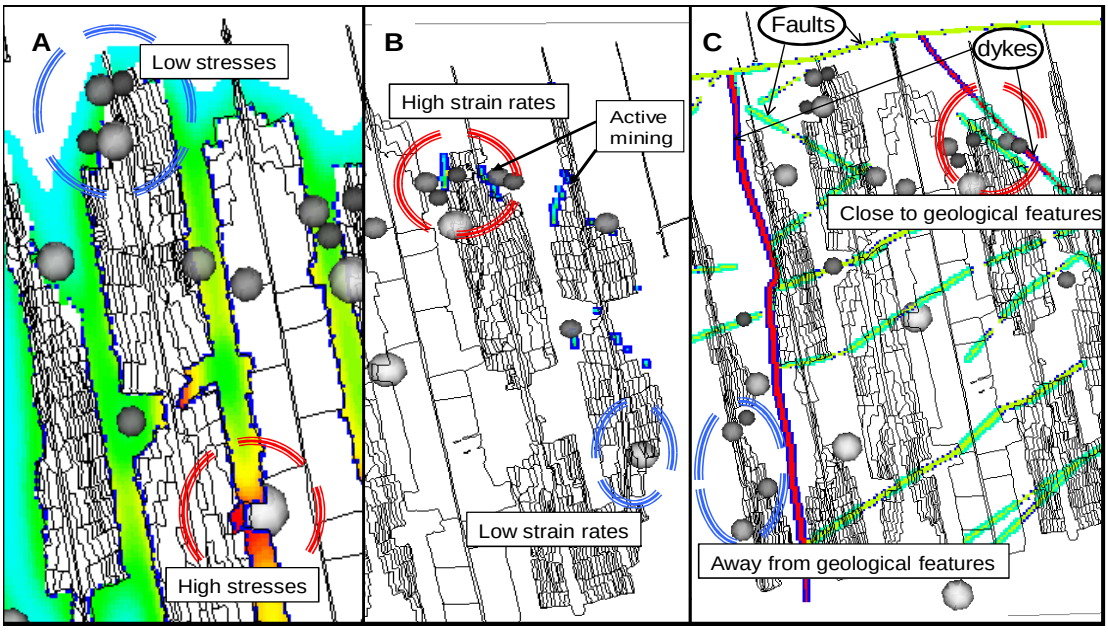

Figure 9.2: Subsets defining three mining conditions. (A) Stress influence (red and blue colour represent high and low stress conditions respectively), (B) Strain rate influence (blue colour represent active mining) and (C) Geological discontinuity influence.

The division of the two mainshock populations is based on the median value giving the condition parameter (e.g. median ERR value of mainshocks). The median is preferred as it divides the mainshocks into equal populations. Figure 9.3 demonstrates the mainshock division based on the median ERR value. Population 1 represents mainshocks locating at high stressed faces and population 2 represents mainshocks locating at low stress faces. Also shown on the figure is the apparent stress of the mainshocks, computed using the equation;

$$\sigma_A = G W_R / M_0 \tag{9.1}$$

Where G = 3.0 $\times 10^{10}$ Pa is the average modulus of rigidity of the rock types at the two reefs (Milev and Spottiswoode, 2002, Spottiswoode et. al., 2008), W_R and M_0 are the released seismic energy and seismic moment of the mainshock. Apparent stress is a measure of the dynamic stress release during the occurrence of an event (Ryder & Jager, 2002, pg 221). Population 1 shows a decrease in apparent stress with increasing ERR, while population 2 shows a constant apparent stress (each data point represents an apparent stress value averaged over 24 mainshocks) with increasing ERR values. The difference in apparent stress between the two populations gives a physical parameter that distinguished the two populations.

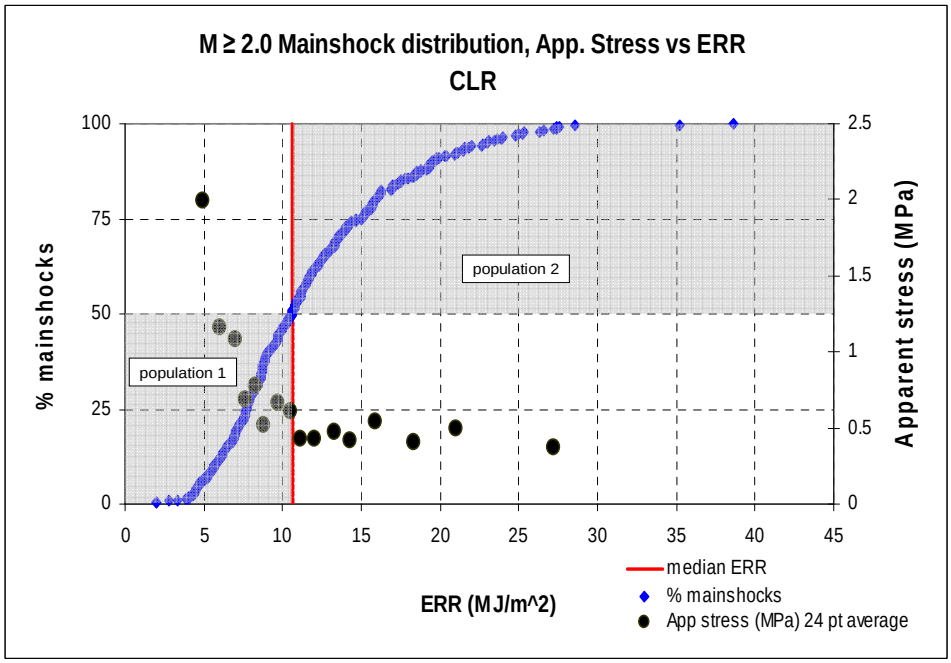

Figure 9.3: Division of mainshocks into two populations to study the influence of geological discontinuities on aftershock productivity.

The median distance of mainshocks from geological features is used to define the two mainshock populations.

In figure 9.3, the two population groups are defined by computing the median ERR value (10.6 MJ/m^2) of the mainshocks. This median ERR value divides the populations into two equal percentages of mainshocks (shaded areas in figure 9.3).

The extraction of rock as mining progresses results in stress redistributions from mined out to un-mined ground. These energy changes lead to high stress concentrations particularly at mining faces. ERR, measured in MJ/m^2 provides a measure of these energy changes and stress concentrations. ERR

generally measures the severity of mining conditions, particularly the stress concentrations at mining faces (Ryder and Jager, 2002, pg. 229,233). In some studies, ERR was found to show a positive correlation with seismicity (Jager and Ryder, 1999, pg. 48).

ERR is calculated by considering the extraction of an area ΔA from a horizontal stope with a resulting volume change ΔV from overlaying strata sag. The change in the potential energy of the overlaying strata is given by $q_v \Delta V$, where q_v is the virgin vertical stress. For mining with no backfill or any considerable support, one-half of the energy change is stored as strain energy in the rockmass. The other half is released in different forms such as shearing and heating. This released energy is called the Energy Release Rate and given by:

$$ERR = \frac{1}{2} q_v \, \Delta V / \Delta A \tag{9.2}$$

Although ERR presents a measure of expected mining conditions, it suffers major shortcoming associated with local geological conditions. ERR is insensitive to geological discontinuities which are often found in the rockmass and are associated with increased levels of seismicity.

9.2 Results and discussions

Following the method by Yang and Ben-Zion (2009), productivity *K* is determined by integrating equation 2.6 and given by the slope of the line (equation 9.3). Linearization of equation 2.5 assumes p=1.

$$N(t) = K[\ln(t+c) - \ln(t_0+c)] \ldots p = 1 \tag{9.3}$$

where t_0 is the initial time.

It was found that the assumption is valid as mine tremor aftershocks have p-values of about 1 (Figure 9.4). The assumption that p=1, is validated by computing the confidence interval of p. The interval is computed by linearising equation 2.6 where logarithms are taken on both sides of the equation. This allows for p to be determined from the slope of the curve using the method of least-squares and the confidence interval to be constructed. The confidence interval of least-squares estimate $\hat{p}$ of the aftershock decay is given by;

$$[\hat{p} - s_{\hat{p}} T_{n-2}, \hat{p} + s_{\hat{p}} T_{n-2}] \tag{9.4}$$

where $s_{\hat{p}}$ is the standard deviation of $\hat{p}$, n is the number of data points and T_{n-2} is the Student's t-value with n-2 degrees of freedom. The standard deviation of $\hat{p}$ is given by;

$$s_{\hat{p}} = \sqrt{\frac{\frac{1}{n-2}\sum_{i=1}^{n}\varepsilon_i^2}{\sum_{i=1}^{n}\left(t_i - \bar{t}\right)^2}} \tag{9.5}$$

where t_i is the time of occurrence of aftershocks, $\bar{t}$ is the mean time of occurrence and ε_i^2 is the square of the residuals of the aftershocks event rate. The computed standard derivation gives a confidence interval of (0.82, 1.19) at the 95% confidence level which validates the assumption.

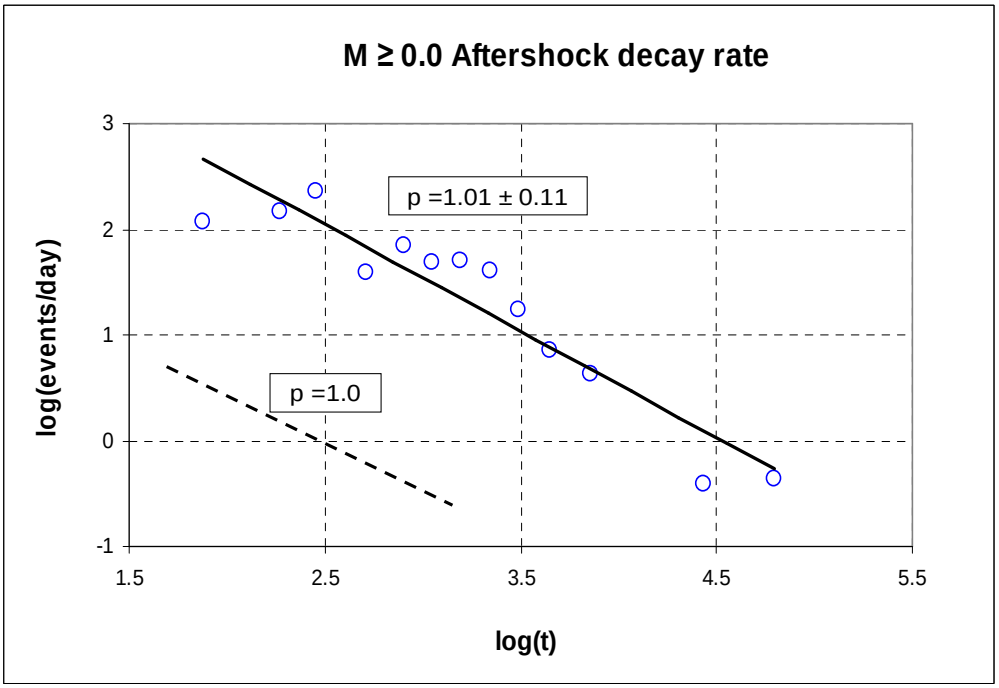

Figure 9.4: M ≥ 0.0 aftershock decay rate following 2.0 ≤ M ≤ 3.0 mainshocks.

Figure 9.5 shows the cumulative seismicity (normalised to the number of mainshocks) used for the determination of *K*. The green curve gives the cumulative data (sum of aftershocks and background data). At later times

(gray area), the background dominates the aftershock data such that equation 9.2 alters to equation 9.6 which includes the background term βt (blue curve).

$$N(t) = K[\ln(t+c) - \ln(t_0 + c)] + \beta t \tag{9.6}$$

The background grows exponentially on the logarithmic scale due to its constant behaviour on a linear scale. To obtain a more confident fit, data is de-trended by removing the long-term average background (blue curve) to obtain the de-trended aftershock data (red curve, Figure 9.5).

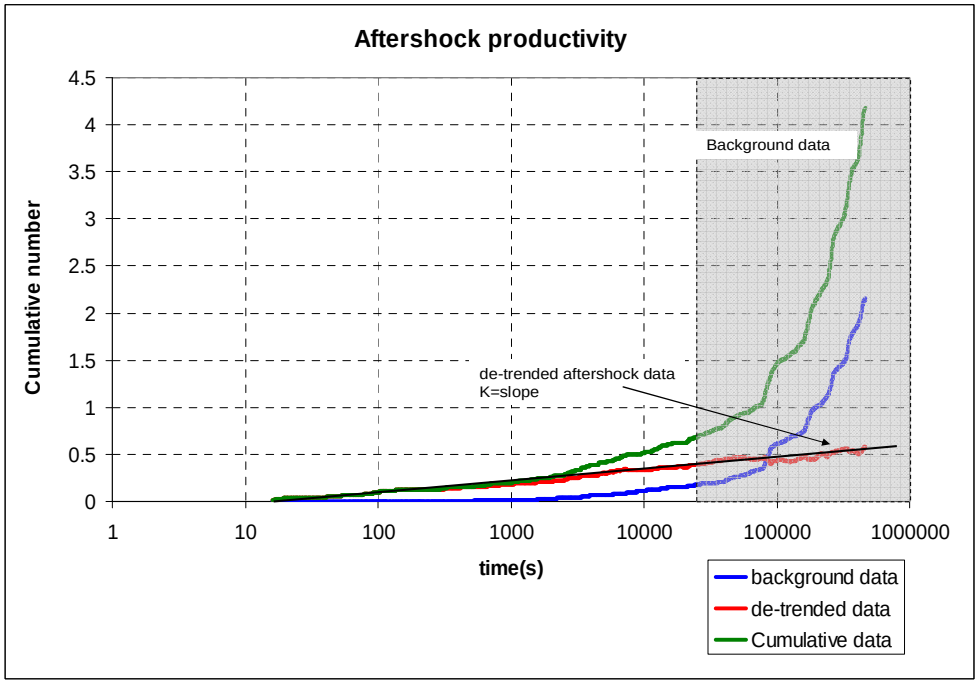

Figure 9.5: Aftershock productivity within 1000 m and 1 day following M ≥ 2.0 mainshocks.

The green curve represents the cumulated data, the blue curve represents the background data and the red curve represents the de-trended aftershock data.

Figure 9.6 shows the comparison of aftershock productivity for high stress versus low stress environments, as measured by ERR. The two mainshock populations are separated from each other based on the median ERR value of 9.4 MJ/m^2 and 10.6 MJ/m^2 for VCR and CLR mines respectively.

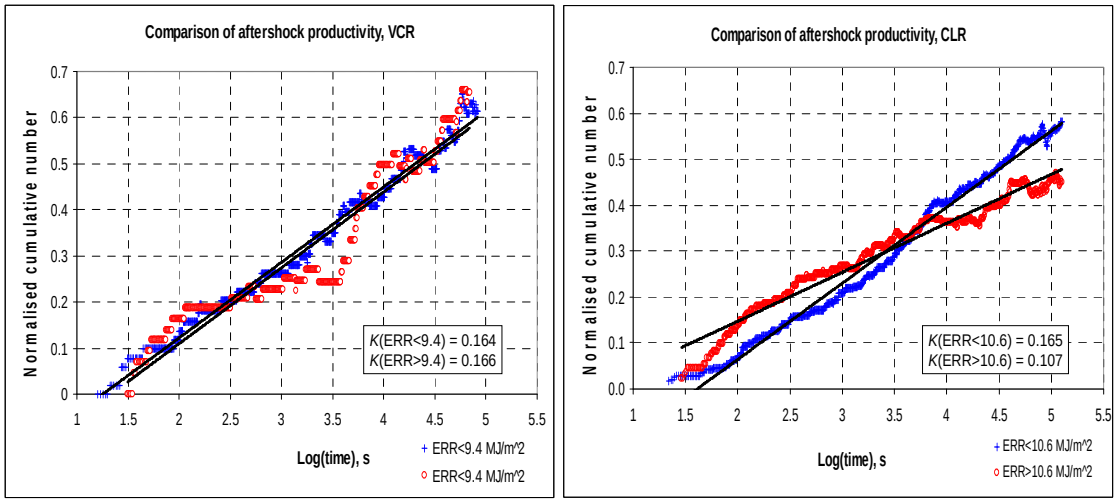

Figure 9.6: Aftershock productivity dependency on stress environments.

Productivity *K*, given by the slopes of the curves shows a similar value for the two contrasting mainshock populations. Figure 9.7 shows a similar relationship between aftershock productivity and proximity to geological features.

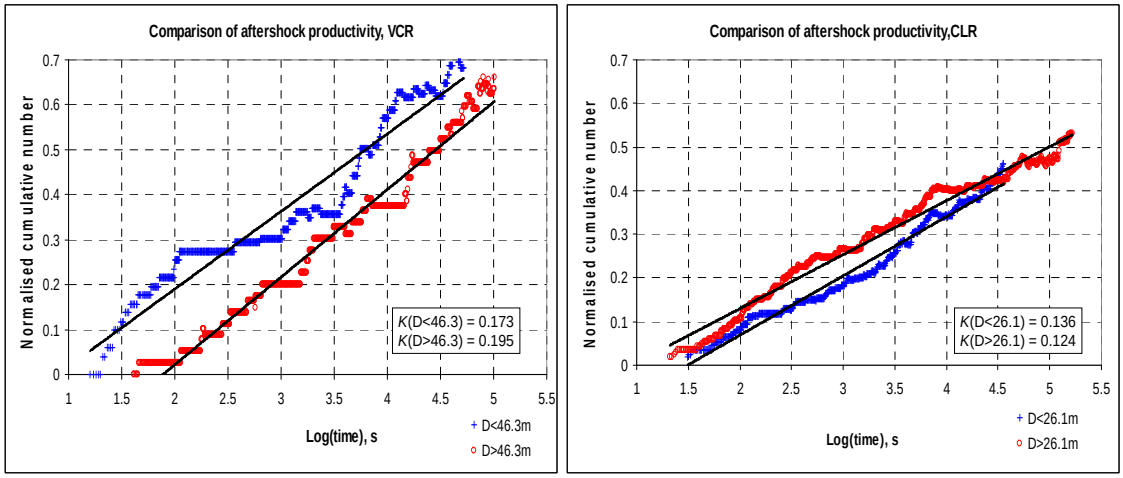

Figure 9.7: Aftershock productivity dependency on geological discontinuities.

Mainshocks near actively mined faces are in a high strain rate environment while mainshocks locating further from actively mined faces or in stationary faces are in a low strain environment. As a proxy for strain rate, the distance to the face (D) was used. This consistency was also noted when considering the dependency of productivity on strain rates (Figure 9.8).

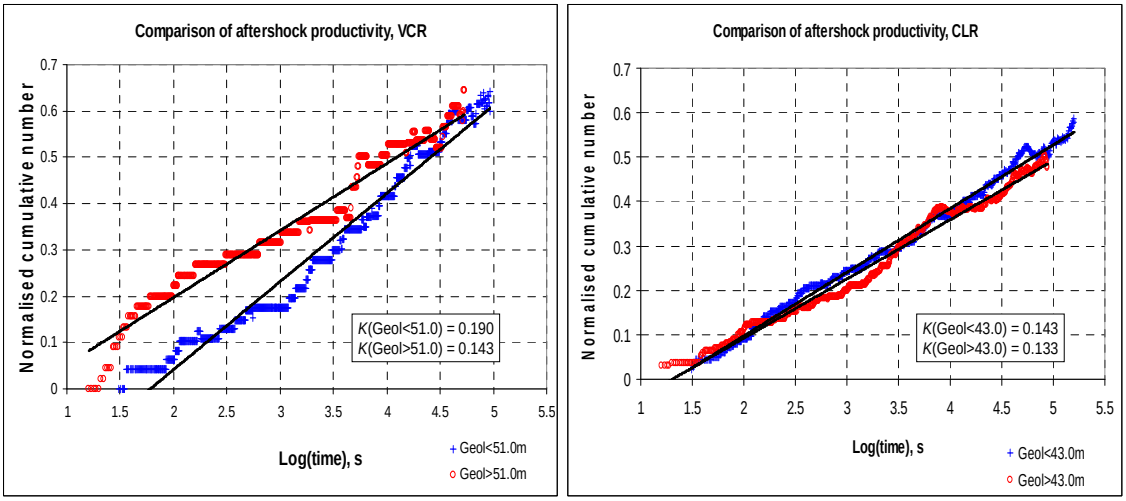

Figure 9.8: Aftershock productivity dependency on strain environments.

To investigate whether the difference in the similar values of the slopes of the contrasting populations are statistically significant, the confidence intervals associated with the least-squares estimate of the productivity *K* are computed. The confidence interval of the least-squares estimate $\hat{K}$ of productivity is computed using the equation similar to 9.3;

$$[\hat{K} - s_{\hat{K}} T_{n-2}, \hat{K} + s_{\hat{K}} T_{n-2}] \tag{9.7}$$

where $s_{\hat{K}}$ is the standard deviation of $\hat{K}$, n is the number of aftershocks and T_{n-2} is the Student's t-value with n-2 degrees of freedom. The standard deviation of $\hat{K}$ is given by;

$$s_{\hat{K}} = \sqrt{\frac{\frac{1}{n-2}\sum_{i=1}^{n} \varepsilon_i^{\,2}}{\sum_{i=1}^{n} \left(x_i - \bar{x} \right)^2}} \tag{9.8}$$

where x_i is the time of occurrence of aftershocks, $\bar{x}$ is the mean time of occurrence of aftershocks and $\varepsilon_i^{\,2}$ is the square of the residuals of the normalized cumulated aftershocks. The table 9.1 summarizes the results of the comparisons. The confidence intervals of the slopes are computed at the 95% confidence level.

Table 9.1: Statistical comparison of aftershock productivity for contrasting mining environments.

Orebody	**VCR**			**CLR**		
	n	95% confidence interval of K		n	95% confidence interval of K	
ERR (MJ/m^2)	643	< 9.4	0.163 ≤ 0.164 ≤ 0.165	769	< 10.6	0.164 ≤ 0.165 ≤ 0.166
	683	> 9.4	0.154 ≤ 0.158 ≤ 0.162	769	> 10.6	0.106 ≤ 0.107 ≤ 0.108
Geol (m)	739	< 51.0	0.188 ≤ 0.190 ≤ 0.192	792	< 43.0	0.142 ≤ 0.143 ≤ 0.144
	684	> 51.0	0.143 ≤ 0.145 ≤ 0.147	733	> 43.0	0.132 ≤ 0.133 ≤ 0.134
D (m)	686	< 46.3	0.170 ≤ 0.173 ≤ 0.176	643	< 26.1	0.135 ≤ 0.136 ≤ 0.137
	748	> 46.3	0.193 ≤ 0.195 ≤ 0.197	796	> 26.1	0.123 ≤ 0.124 ≤ 0.125

Comparisons based on the confidence intervals of the slopes show that although the productivity is not highly influenced by the mining environment, the productivity is however statistically different when compared at a 95% confidence level. Productivity of mainshocks locating in environments with values less than the median value of the parameter tend to have a significantly higher slope. The only exception is the comparison between the slopes of the strain environments at the VCR where the slope is higher for mainshocks locating further away from actively mined faces.

The results obtained are rather unexpected as they suggest that the number of aftershocks following a mainshock is not highly dependant on the conditions of which the mainshocks locates. As an example, the results imply that approximately the same number of aftershocks will follow the mainshock

whether the mainshock locates far from or in close proximity to geological features.

Productivity can also be measured as the proportion of aftershocks in the entire recorded seismic catalogue. To measure what percentage of the seismic catalogue are aftershocks, aftershock proportion is determined with reference to the 3× and 10× background rates. Equation (9.9) is used to determine the aftershock proportion.

$$P = \frac{N_A(t_A)}{N_{total}} \tag{9.9}$$

Where t_A is the time taken for the aftershock decay rate to reach 3× and 10× the background rate, N_A is the number of aftershocks occurring within t_A and N_{total} is the total number of seismic events in the catalogue (Table 3.1). The following tables give the proportion of aftershocks in the total catalogue with reference to the 3× and 10× the background rates.

Table 9.2 : Proportion of aftershocks (VCR mine)

1.0 ≤ M ≤ 2.0	**N_A(tA)**	**Proportion of aftershocks (%)**
3 × BG	124	0.96
10 × BG	67	0.55
2.0 ≤ M ≤ 3.0		
3 × BG	88	0.40
10 × BG	47	0.23
3.0 ≤ M ≤ 4.0		
3 × BG	39	0.15
10 × BG	22	0.12

Table 9.3: Proportion of aftershocks (CLR mine)

1.0 ≤ M ≤ 2.0	**N_A(tA)**	**Proportion of aftershocks (%)**
3 × BG	198	1.21
10 × BG	114	0.65
2.0 ≤ M ≤ 3.0		
3 × BG	84	0.86
10 × BG	49	0.46
3.0 ≤ M ≤ 4.0		
3 × BG	31	0.38
10 × BG	25	0.21

Table 9.3 shows that for 2.0 ≤ M ≤ 3.0 mainshocks, 0.86 % of the seismic events are aftershocks with reference to the 3 × the background rate. For 3.0 ≤ M ≤ 4.0 mainshocks, 0.38 % of the seismic events are aftershocks with

reference to the 3 × the background rate. A practical implication for these tables would be for example, if re-entry times are postponed until the hazard declines to 3 × the background reference levels, then 0.86 % of the seismic hazard posed by aftershocks would be avoided.

9.3. Conclusions

Unexpectedly, aftershock productivity shows no dependency on the three mining conditions investigated. This is shown by a similar value of the slope of the curves (giving the aftershocks productivity) compared for the two contrasting populations. Although the statistical comparison shows a significant difference between the productivity of the contrasting mainshocks when compared at the 95% confidence level, productivity is not highly influenced by these mining parameters. These results are unexpected when considering the fact that seismicity depends on ERR, strain rates and geological discontinuities and that mining close to geological structures tend to increase the level of seismicity (Jager and Ryder, 1999, pg 51).

CHAPTER 10. CONCLUSIONS AND FURTHER RESEARCH

A methodology of accessing the seismic hazard posed by aftershock following larger seismic events has been developed by consideration of statistical and deterministic analysis of mine tremor aftershocks. Statistical analysis considered the statistical properties of aftershocks. Mine tremor aftershocks obeyed the empirical relations; Gutenberg-Richter frequency-magnitude, Modified Omori law and the density law, same as natural earthquakes do. However, Båth's law was violated and the violation found to be manifested in the mining geometry, particularly the panel length. It was also found that generally the mining geometry also tends to limit the maximum aftershock magnitude to less than 4.0, as shown by the frequency-magnitude relation analysis.

Deterministic analysis was performed in order to study the dependency of mine tremor aftershocks on mining conditions (stresses, strain rates and proximity to geological features (faults and dykes)), particularly the productivity. It was found that aftershock productivity is not highly influenced by local stresses, strain rates and proximity to geological features.

Using the statistical properties of aftershocks, time periods following the mainshocks where the seismic hazard has decreased to background levels were estimated. These time periods can be used to postpone re-entry to

working areas following the evacuation of underground personnel after the occurrence of a larger seismic event. In the case where the event occurs while people are in their working areas, it is recommended that people should take cover at safer areas or closest support structures.

Further research is needed in understanding the physical mechanisms governing aftershock generation and triggering. Phenomenon like the bi-modal nature (two different b-values for the same dataset) of mine events still requires further research and understanding of the physics behind its occurrence. Understanding of stress perturbations due to the mainshock also needs further research in order to give insight to aftershock triggering mechanisms in the near and far fields.

REFERENCES

Aki, K., A probabilistic synthesis of precursory phenomenon, Earthquake prediction-International review, Maurice Ewing Volume, *American Geophysical Union*, 1981, pp. 566-574.

Aki, K., Maximum likelihood estimate of the b value in the formula log N = a - bM and its confidence limits, *Bulletin of the Earthquake Research Institute*, 43, 1965, pp. 273-239.

Båth, M., Lateral inhomogeneities in the upper mantle, *Tectonophysics*, 2, 1965, pp. 483-514.

Brady, B. H. G., and Brown, E. T., *Rock Mechanics for Underground Mining*, New York, Lower Academic Publishers, 2005.

Console, R., Lombardi, A. M., Murrow, M., and Rhoades D., Båth's law and the self-similarity of earthquakes, *Journal of Geophysical Research*, 108, 2003, pp. 2128, doi 10.1029/2001JB001651.

Durrheim, R. J., Roberts, M. K. C., Haile, A. T., Hagan, T, O., Jager, A. J., Handley, M. F., Spottiswoode, S. M., and Ortlepp, W. D., Factors influencing the severity of the rockburst damage in South African gold mines, *The Journal of The South African Institute of Mining and Metallurgy*, March/April 1998, pp. 53-57.

Felzer, K. R., and Brodsky, E. E., Decay of aftershock density with distance indicates triggering by dynamic stress, *Nature*, 441, 2006, pp. 735-738.

Freed, A, M., Earthquake triggering by static, dynamic, and postseismic stress transfer, *Annual Review of Earth and Planet Sciences*, 33, 2005, pp. 335-367.

Frolich, C., and Davis, S. D., Teleseismic b-values; or, much ado about 1.0, *Journal of Geophysical Research*, 98. B1, 1993, pp 631-644.

Ganas, A., Gosar, A., and Drakatos, G., Static stress changes due to the 1998 and 2004 Krn Mountain (Slovenia) earthquakes and implications for future seismicity, *Natural Hazards and Earth System Sciences*, 8, 2008, pp. 59-66.

Gibowicz, S. J., Stress drop and aftershocks, *Bulletin of Seismological Society of America*, 63, 4, 1973, pp. 1433-1446.

Gibowicz, S. J., and Kijko, A., *An Introduction to Mining Seismology*, California: Academic Press, Inc, 1994.

Gross S. J., and Kisslinger C., Tests of models of aftershock rate decay, *Bulletin of the Seismological Society of America*, 84, 5, 1994, pp.1571-1579.

Gutenberg, B., and Richter, C. F., *Seismicity of the Earth and Associated Phenomenon*, 2nd ed. Princeton, Princeton Univ. Press, 1954.

Guttorp, P., On least squares estimation of b values, *Bulletin of the Seismological Society of America*, 77, 6, 1987, pp. 2115-2124.

Hill, P. D., Dynamic triggering, *Treatise in Geophysics*, 4, 2007, pp. 257-291.

Jager, A. J., and Ryder, J. A., *A Handbook on Rock Engineering Practice for Tabular Hard Rock Mines*, Braamfontein: SIMRAC, 1999.

Kagan, Y. Y., Short-term properties of earthquake catalogues and models of earthquake sources, *Bulletin of the Seismological Society of America*, 94, 4, 2004, pp. 1207-1228.

Kgarume, T. E., Spottiswoode, S. M., and Durrheim, R. J., Statistical properties of mine tremor aftershocks, *Pure and Applied Geophysics*, 167, 2010, pp. 107-117.

Kgarume T. E., Spottiswoode S. M., and Durrheim, R. J., Deterministic properties of mine tremor aftershocks, *5th International Seminar on Deep and High Stress Mining*, Santiago Chile, October 2010 (In press).

Kgarume, T., and Spottiswoode, S. M., Density and rate of mine aftershocks and the implications for seismic hazard assessment, *Proceedings of the Annual Africa Array workshop*, Jul. 2008.

Kgarume, T., and Spottiswoode, S. M., Analysis of aftershock decay rates of mine seismic events, *Proceedings of the Biannual South African Geophysical Association*, Sep. 2007.

Legge, N., and Spottiswoode S. M., Fracturing and micro-seismicity ahead of a deep gold mine stope in the pre-remnant and remnant stages of mining, *6th Congress of the International Society of Rock Mechanics*, Herget G., and Vongpaisal S., (eds), Rotterdam Netherlands, 1987, pp. 1071-1077.

Madariaga, R., Dynamics of an expanding circular fault, *Bulletin of the Seismological Society of America*, 66, 3, 1976, pp. 639-666.

Malan, D. F., Time-dependent behaviour of deep level tabular excavations in hard rock, *Rock Mechanics and Rock Engineering*, 32, 2, 1999, pp. 123-155.

Malan, D. F., A viscoelastic approach of the modelling of the transient closure behaviour of tabular excavations after blasting, *The Journal of The South African Institute of Mining and Metallurgy*, Sep. 1995, pp. 211-220.

McCarthy, T. S., The Witwatersrand Supergroup, In: Johnson, M. R., Anhaeusser, C. R., and Thomas, R. J., (Eds.), *The Geology of South Africa*, Geological Society of South Africa, Johannesburg and The Council for Geosciences, Pretoria, South Africa, 2006.

McGarr, A., Some applications of seismic source mechanism studies to assessing underground hazard, *Proceedings of the 1st International Congress on Rockbursts and Seismicity in Mines*, Johannesburg, SAIMM, 1984, pp. 199-208.

McGarr, A., Spottiswoode, S. M., and Gay, N. C., Relationship of mine tremors to induced stresses and to rock properties in the focal region, *Bulletin of the Seismological Society of America*, 65, 4, 1975, pp. 981-993.

Mendecki, A. J., *Seismic Monitoring in Mines*, London: Chapman & Hall, 1997.

Milev, A. M., and Spottiswoode, S. M., Effect of rock properties on mining-induced seismicity around the Ventersdorp Contact Reef, Witwatersrand Basin, South Africa, *Pure and Applied Geophysics*, 159, 2002, pp. 165-177.

Nanjo, K., Nagahama, H., and Satomura, M., Rates of aftershock decay and the fractal structure of active fault systems, *Tectonophysics*, 287, 1998, pp. 173-186.

Omori, F., On the aftershocks of earthquakes, *Journal of the College of Science,* Imperial University of Tokyo, Japan, 7, 1894, pp. 111-200.

Persh, S., and Houston, H., Strongly depth-dependent aftershock production in deep earthquakes, *Bulletin of the Seismological Society of America*, 94, 5, 2004, pp. 1808-1816.

Pollitz, F. F., and Sacks, I. S., Stress triggering of the 1999 Hector mine earthquake by transient deformation following the 1992 Landers earthquake, *Bulletin of the Seismological Society of America*, 92, 4, 2002, pp. 1487-1496.

Reasenberg, P. A., and Jones, L. M., Earthquake hazard after a mainshock in California, *Science*, 243, 1989, pp. 1173-1176.

Richardson, E., and Jordan, T. H., Seismicity in the gold mines of South Africa: Implications for tectonic earthquakes, *Bulletin of the Seismological Society of America*, 92, 5, 2002, pp. 1766–1782.

Richter, C. F., An instrumental earthquake scale, *Bulletin of the Seismological Society of America*, 25, 1, 1935, pp. 1-32.

Robb, L. J., and Robb, V. M., Gold in the Witwatersrand basin, In: Wilson, M. G. C., and Anhaeusser, C. R., (Eds.), *Mineral Resources of South Africa*, Council for Geoscience, Pretoria, South Africa, 1998.

Ryder, J. A., and Jager, A. J., *A Handbook on Rock Mechanics for Tabular Hard Rock Mines*, Braamfontein: SIMRAC, 2002.

Shcherbakov, R., Turcotte, D. L., and Rundle, J. B., Aftershock statistics, *Pure and Applied Geophysics*, 165, 2005, pp. 1051-1076.

Shcherbakov, R., Turcotte, D. L., and Rundle, J. B., Scaling properties of the Parkfield aftershock sequence, *Bulletin of the Seismological Society of America*, 96, 4B, 2006, pp. S376-S384.

Sellers, E. J., Kataka, M., Singh, N., Ebrahim-Trollope, R., Handley, R., Milev, A., Spottiswoode, S., *New methodologies for quantifying remnant*

extraction hazards in deep mines, Safety In Mines Research Advisory Committee (SIMRAC) report, SIM 020303, 1995, pp.180.

Scholz, H. C., *The Mechanisms of Earthquakes and Faulting*, Cambridge, Cambridge Univ. Press, 1990.

Spottiswoode, S. M., Linzer, L. M., and Majiet, S., *Energy and stiffness of mine models and seismicity*, In SHIRMS 2008, Potvin, Y., Carter, J., Dyskin, A., Jeffrey, R., (eds), Australian Centre for Geomechanics, Perth, ISBN 978-0-9804185-5-2, 1, 2008, pp. 693-707.

Spottiswoode, S. M., and Linzer, L. M., *Improved seismic locations and location techniques*, Safety In Mines Research Advisory Committee (SIMRAC) report Appendix I, SIM 020304, 2006, pp. 65.

Spottiswoode, S. M., and Milev A. M., *A methodology and computer program for applying improved, inelastic ERR for the design of mine layouts on planar reefs*, Safety In Mines Research Advisory Committee (SIMRAC) report, GAP 722, 2002.

Spottiswoode, S. M., Aftershocks and foreshocks of mine seismic events, *3rd International Workshop on the Application of Geophysics to Rock and Soil Engineering*, GeoEng2000, Melbourne Australia, 2000.

Spottiswoode, S. M., and McGarr, A., Source parameters of mine tremors in a deep-level gold mine, *Bulletin of the Seismological Society of America*, 65,1, 1975, pp. 93-112.

Stein, R. S., The role of stress transfer in earthquake occurrence, *Nature*, 402, 1999, pp. 605-609.

Stein, R. S., and Lisowski, M., The 1979 Homestead Valley earthquake sequence, California: control of aftershocks and postseismic deformation, *Journal of Geophysical Research*, 88, B8, 1983, pp. 6477-6490.

Turcotte, L. D., *Fractals and Chaos in Geology and Geophysics*. 2nd ed. Cambridge, Cambridge Univ. Press, 1997.

Utsu, T., A statistical study on the occurrence of aftershocks, *Geophysics Magazine*, 30, 1961, pp. 521-605.

Vere-Jones, D., A note on the statistical interpretation of Båth's Law, *Bulletin of the Seismological Society America*, 59, 1969, pp. 1535-1541.

Yang, W., and Ben-Zion, Y., Observational analysis of correlations between aftershock productivities and regional conditions in the context of a damage rheology model, *Geophysical Journal International*, 177, 2009, pp. 481-490.